$H_3)_3$ proceeded in a manner which was entirely different from that of $B_3H_6{\cdot}2P(CH_3)_3{}^+B_3H_8{}^-$. The latter compound reacted with $N(CH_3)_3$ and gave the tetraborane(8) adduct $B_4H_8{\cdot}P(CH_3)_3{\cdot}N(CH_3)_3$.[15] In contrast, the treatment of $B_3H_6{\cdot}2N(CH_3)_3{}^+B_3H_8{}^-$ with $N(CH_3)_3$ (1:2 molar ratio) at −20 °C resulted in the abstraction of a BH_3 unit from the cation; the $B_3H_8{}^-$ anion remained intact. Thus another new diboron complex cation, $B_2H_3{\cdot}3N(CH_3)_3{}^+$, was produced.[16] See the second step in Scheme I. The ^{11}B NMR signals of this diboron cation appeared as broad humps at 12.5 and −3.9 ppm with the half-height widths 300 and 450 Hz, respectively.

Thus, the isolation of $B_2H_4{\cdot}2N(CH_3)_3$ not only has filled the vacancy in the list of representative compounds but also has given an additional insight into the roles of different Lewis base ligands that are responsible for subtle reactivity differences of borane adducts. Further work on the derivative chemistry of $B_2H_4{\cdot}2N(CH_3)_3$ is being pursued, and the details of the results will be reported at a later date.

Acknowledgment. We acknowledge support of this work by the U.S. Army Research Office through Grant DAAG 29-85-K-0034.

Registry No. $B_3H_7{\cdot}THF$, 52842-96-3; $BH_3{\cdot}N(CH_3)_3$, 75-22-9; $B_2H_4{\cdot}2N(CH_3)_3$, 97551-45-6; $B_2H_4{\cdot}N(CH_3)_3{\cdot}P(CH_3)_3$, 97551-46-7; $B_2H_4{\cdot}2PMe_3$, 67113-98-8; $B_3H_7{\cdot}N(CH_3)_3$, 57808-48-7; $BH_2Cl{\cdot}N(CH_3)_3$, 5353-44-6; $B_2H_7{}^-$, 27380-11-6; $B_3H_8{}^-$, 12429-74-2; B_2H_6, 19287-45-7; B_4H_{10}, 18283-93-7; $B_2H_3{\cdot}3N(CH_3)_3{}^+$, 97551-47-8.

Department of Chemistry
University of Utah
Salt Lake City, Utah 84112

Rosemarie E. DePoy
Goji Kodama*

Received April 29, 1985

(15) Kameda, M.; Kodama, G. *Inorg. Chem.* **1984**, *23*, 3705.
(16) Another diboron complex cation, $B_2H_5{\cdot}2P(CH_3)_3{}^+$, has been synthesized [Kameda, M.; Kodama, G. "Abstracts of Papers", 40th Northwest Regional Meeting of the American Chemical Society, Sun Valley, ID, June 1985; No. 59].

Articles

Contribution from the Faculty of Chemistry, University of Bielefeld, D-4800 Bielefeld, West Germany

Synthetic, Spectroscopic, X-ray Structural, and Quantum-Chemical Studies of Cyanothiomolybdates with Mo_2S, Mo_2S_2, Mo_3S_4, and Mo_4S_4 Cores: A Remarkable Class of Species Existing with Different Electron Populations and Having the Same Central Units as the Ferredoxins

A. MÜLLER,*[1a] R. JOSTES,[1a] W. ELTZNER,[1a] CHONG-SHI NIE,[1a,b] E. DIEMANN,[1a] H. BÖGGE,[1a] M. ZIMMERMANN,[1a] M. DARTMANN,[1a] U. REINSCH-VOGELL,[1a] SHUN CHE,[1a,c] S. J. CYVIN,[1d] and B. N. CYVIN[1d]

Received June 26, 1984

Spectroscopic (IR, Raman, resonance Raman, electronic absorption, photoelectron (XPS)) properties of the cyanothiomolybdates $[Mo_4S_4(CN)_{12}]^{8-}$ (**1**), $[Mo_3S_4(CN)_9]^{5-}$ (**2**), $[Mo_2S_2(CN)_8]^{6-}$ (**3**), $[Mo_2S_2(CN)_8]^{4-}$ (**4**), and $[Mo_2S(CN)_{12}]^{6-}$ (**5**) (which might have been of importance for the evolution of Mo enzymes and for the prebiotic evolution in general) have been investigated and discussed on the basis of EH–SCCC–MO calculations. The complexes (with central units comparable to those of the ferredoxins) exist with different electron populations. The preparations of $K_5[Mo_3S_4(CN)_9]{\cdot}2H_2O$ (**2a**) (obtained by extrusion from MoS_3), $[(C_6H_5)_4P]_4[Mo_2S_2(CN)_8]{\cdot}2H_2O$ (**4a**), and the related compound $K_6[Mo_2S_2(NO)_2(CN)_6]{\cdot}4H_2O$ (**6a**) are reported as well as the X-ray structures of $K_5[Mo_3S_4(CN)_9]{\cdot}3KCN{\cdot}4H_2O$ (**2b**) and $[(C_6H_5)_4P]_4[Mo_2S_2(CN)_8]{\cdot}nH_2O$ (**4b**) and the indexed powder diffraction data of $K_8[Mo_4S_4(CN)_{12}]{\cdot}4H_2O$ (**1a**). Salts of **1** and **2** can be directly prepared by reaction of MoS_3 with CN^- in aqueous solution. **2b** crystallizes in the monoclinic space group *Cm* (*Z* = 2): *a* = 15.661 (3) Å, *b* = 18.807 (3) Å, *c* = 6.552 (1) Å, and β = 116.39 (1)°. On the basis of 1985 unique data ($F_o > 3.92\sigma(F_o)$, θ–2θ scan) the structure was refined to *R* = 3.1%. The central $[Mo_3S_4]$ unit of the anion **2** (idealized symmetry C_{3v}) can be described as an incomplete distorted cube (d_{av}(Mo–Mo) = 2.773 Å, d_{av}(Mo–(μ-S)) = 2.322 Å, d_{av}(Mo–(μ_3-S)) = 2.361 Å) with pseudooctahedral coordination of the Mo atoms (three bridging S atoms and three cyano ligands; d_{av}(Mo–C) = 2.210 Å, d_{av}(C–N) = 1.136 Å). **4b** crystallizes in the orthorhombic space group *Pnna* (*Z* = 4): *a* = 29.871 (21) Å, *b* = 24.278 (26) Å, and *c* = 13.405 (11) Å. On the basis of 1868 unique data ($F_o > 3.92\sigma(F_o)$, ω scan) the structure could only be refined to *R* = 15.7% (due to the poor quality of crystals). The anion **4** (idealized symmetry D_{2h}) contains planar $Mo(S_{br})_2Mo$ units (*d*(Mo–Mo) = 2.758 (7) Å, d_{av}(Mo–S) = 2.296 Å) with pseudooctahedral coordination of the Mo atoms (two bridging S atoms and four cyano ligands; d_{av}(Mo–C) = 2.12 Å, d_{av}(C–N) = 1.18 Å). For the highly symmetrical **1** a detailed vibrational analysis including an approximate normal-coordinate analysis has been performed.

Introduction

Cyanothiomolybdates seem to have been of importance for the evolution of Mo enzymes and for the prebiotic evolution in general.[2-5] We were able to show that species with different electron populations having the same (or roughly the same) central units as the ferredoxins (2 Fe, 3 Fe, 4 Fe type) can be prepared, and some of these even under possible prebiotic conditions (e.g., by reaction of aqueous CN^- with MoS_x phases). A very remarkable one is the tetranuclear species $[Mo_4S_4(CN)_{12}]^{8-}$ (**1**)[6] with an Mo_4S_4 cube and with T_d symmetry. The other complexes under

(1) (a) University of Bielefeld. (b) Permanent address: Shanghai Institute of Organic Chemistry, Academica Sinica, 345 Linglin Lu, Shanghai, China. (c) Permanent address: Dalian Institute of Chemical Physics, Academica Sinica, Dalian, China. (d) Institute of Physical Chemistry, University of Trondheim, Trondheim, Norway.
(2) H. Follmann, "Chemie and Biochemie der Evolution", Quelle und Meyer, Heidelberg, 1981, pp 45, 67.
(3) M. T. Beck and J. Ling. *Naturwissenschaften*, **64**, 91 (1977); cf. also M. T. Beck, *Met. Ions Biol. Syst.*, **7** (1978).
(4) P. C. H. Mitchell and C. F. Pygall, *J. Inorg. Biochem.*, **11**, 25 (1979).
(5) A. Müller, E. Diemann, R. Jostes, and H. Bögge, *Angew. Chem.*, **93**, 957 (1981); *Angew. Chem., Int. Ed. Engl.*, **20**, 934 (1981).
(6) A. Müller, W. Eltzner, H. Bögge, and R. Jostes, *Angew. Chem.*, **94**, 783 (1982); *Angew. Chem., Int. Ed. Engl.*, **21**, 789 (1982); *Angew. Chem. Suppl.*, 1643 (1982).

0020-1669/85/1324-2872$01.50/0

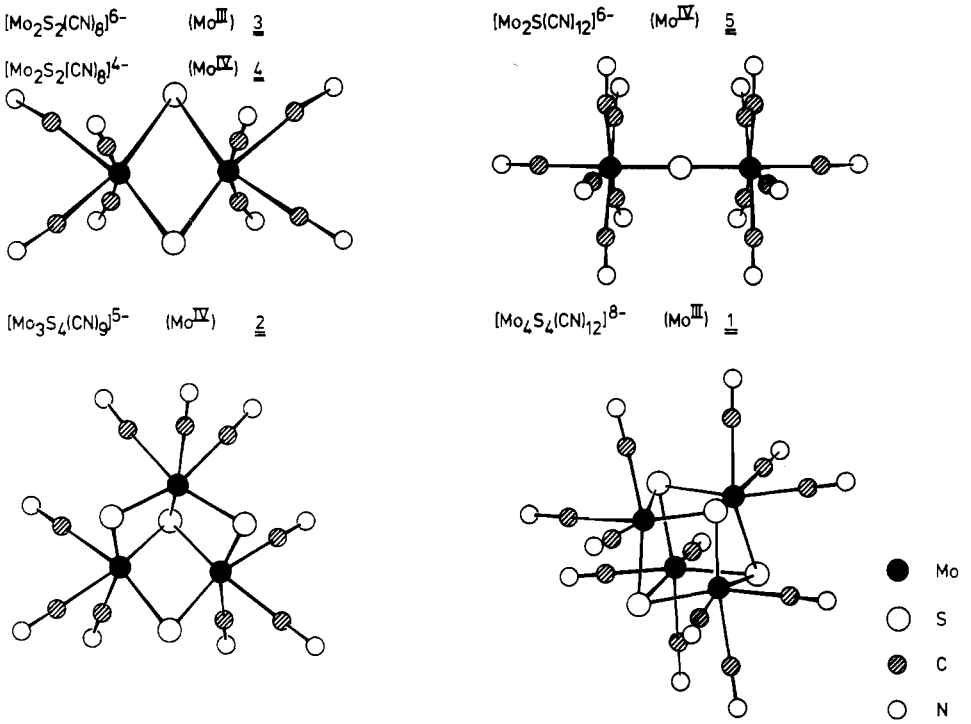

Figure 1. Cyanothiomolybdates with central di-, tri-, and tetranuclear units and different electron populations.

investigation are $[Mo_3S_4(CN)_9]^{5-}$ (**2**),[7] $[Mo_2S_2(CN)_8]^{6-}$ (**3**),[8-11] $[Mo_2S_2(CN)_8]^{4-}$ (**4**), and $[Mo_2S(CN)_{12}]^{6-}$ (**5**).[12] In this paper we wish to report synthetic, spectroscopic, and structural studies of the highly symmetrical **1** and of the other cyanothiomolybdates, the structures of which are presented in Figure 1.

Experimental Section

Preparation of Compounds. The following compounds have been prepared as described in the literature: $K_5[Mo_3S_4(CN)_9]\cdot 3KCN\cdot 4H_2O$ (**2b**),[7,13] $K_6[Mo_2S_2(CN)_8]\cdot 4H_2O$ (**3a**),[8,9,11] $K_6[Mo_2S(CN)_{12}]\cdot 4H_2O$ (**5a**),[12] $K_8[Mo_4S_4(NO)_4(CN)_8]\cdot 4H_2O$,[14] $Mo_2S_4(dtc)_2$,[15] $[(C_6H_5)_4P]_2[Mo_2(S_2)_6]$.[16]

$K_5[Mo_3S_4(CN)_9]\cdot 2H_2O$ (2a) and $K_8[Mo_4S_4(CN)_{12}]\cdot 4H_2O$ (1a). A suspension of 5 g of amorphous MoS_3 (which was prepared by acid hydrolysis of $(NH_4)_2MoS_4$) in an aqueous solution of 15 g of KCN (100-mL Erlenmeyer flask covered with a watch glass) is heated to 60 °C for about 30 min. After filtration, the green solution is kept at 60 °C for about 3–4 days. (After that time, the volume of the solution should be 10–15 mL.) Dark red crystals of **1a** separate, which are filtered off and washed successively with 60% aqueous methanol, methanol, and diethyl ether; yield 0.25 g. Anal. Calcd for $K_8[Mo_4S_4(CN)_{12}]\cdot 4H_2O$: Mo, 31.7; S, 10.6; C, 11.9; N, 13.9; H, 0.7. Found: Mo, 32.3; S, 10.3; C, 11.8; N, 13.3; H, 0.6.

After the filtrate is kept at 60 °C for a further 4–5 days dark green, octahedrally shaped crystals of $K_5[Mo_3S_4(CN)_9]\cdot KHCOO\cdot KSCN\cdot 3H_2O$ (**2c**)[17] (yield ca. 3 g) separate together with some byproducts (KSCN, KHCOO, $K_4[Mo(CN)_8]$). The pure **2a** is obtained by successive precipitation from aqueous solutions of the green crude product by addition of methanol/diethyl ether mixtures until no characteristic bands of the impurities are observed in the IR spectrum (yield ca. 2 g). In a similar way, **2a** can be obtained from $K_5[Mo_3S_4(CN)_9]\cdot m KCN\cdot n H_2O$ (m = 0–3, n = 2–4).[7] Anal. Calcd for $K_5[Mo_3S_4(CN)_9]\cdot 2H_2O$: Mo, 32.6; S, 14.5; C, 12.3; N, 14.3; H, 0.5. Found: Mo, 31.6; S, 14.4; C, 12.3; N, 14.4; H, 0.4.

$[(C_6H_5)_4P]_4[Mo_2S_2(CN)_8]\cdot 2H_2O$ (4a). A 1.5-g sample of $[(C_6H_5)_4P]Cl$ and 0.7 g of freshly prepared **3a** are dissolved in 40 mL of water with stirring. After 3 mL of acetic acid (50%) is added, a green crude product precipitates (this precipitation can be completed by passing air or oxygen through the solution), which is sucked off, washed several times with water, and dried in a desiccator under nitrogen; yield 1.9 g. The crude product is purified by extracting it five times with 50-mL portions of dry and hot acetone for 10 min; yield 1.5 g. (The byproducts are soluble in hot acetone.) Suitable crystals of $[(C_6H_5)_4P]_4[Mo_2S_2(CN)_8]\cdot n H_2O$ (**4b**) for X-ray structure analysis were obtained in very low yield in the form of bluish green platelets by slow evaporation of a solution of the purified compound in a dichloromethane/acetone (3:2) mixture under a nitrogen stream. Anal. Calcd for $[(C_6H_5)_4P]_4[Mo_2S_2(CN)_8]\cdot 2H_2O$: C, 67.2; H, 4.5; N, 6.0; S, 3.4; P, 6.7. Found: C, 66.5; H, 4.6; N, 5.7; S, 3.9; P, 6.5.

$K_6[Mo_2S_2(NO)_2(CN)_6]\cdot 4H_2O$ (6a). A 1-g amount of $NH_4K[Mo_4(NO)_4(S_2)_6O]\cdot 2H_2O$[18] and 10 g of KCN are dissolved in 20 mL of water (50-mL Erlenmeyer flask covered with a watch glass) and heated for approximately 4 h to ca. 60 °C. The yellow precipitate of $K_6[Mo_2S_2(NO)_2(CN)_6]\cdot 4H_2O$ is filtered off and washed with 50% aqueous methanol and diethyl ether; yield 0.6 g. Anal. Calcd for $K_6[Mo_2S_2(NO)_2(CN)_6]\cdot 4H_2O$: C, 9.2; H, 1.0; N, 14.4; S, 8.2; K, 30.1. Found: C, 9.2; H, 0.8; N, 14.0; S, 7.8; K, 29.5.

By the same procedure, but under more dilute conditions (50 mL of aqueous solution), orange-red crystals of $K_8[Mo_4S_4(NO)_4(CN)_8]\cdot 4H_2O$ can be isolated.[14]

(7) A. Müller and U. Reinsch, *Angew. Chem.*, **92**, 69 (1980); *Angew. Chem., Int. Ed. Engl.*, **19**, 72 (1980).
(8) E. Crepaz, *Gazz. Chim. Ital.*, **58**, 391 (1928).
(9) P. Christophliemk, Diplomarbeit, University of Göttingen, 1969.
(10) M. G. B. Drew, P. C. H. Mitchell, and C. F. Pygall, *Angew. Chem.*, **88**, 855 (1976); *Angew. Chem., Int. Ed. Engl.*, **15**, 784 (1976).
(11) M. G. B. Drew, P. C. H. Mitchell, and C. F. Pygall, *J. Chem. Soc., Dalton Trans.*, 1213 (1979).
(12) A. Müller and P. Christophliemk, *Angew. Chem.*, **81**, 752 (1969); *Angew. Chem., Int. Ed. Engl.*, **8**, 753 (1969).
(13) The simple preparation method (educt: $Mo_3S_{13}^{2-}$) described in ref 7 leads to $K_5[Mo_3S_4(CN)_9]\cdot m KCN\cdot n H_2O$ (m = 0–3, n = 2–4). Thick needlelike crystals of **2b** (m = 3, n = 4) that are suitable for X-ray analysis could be obtained by mechanical selection from the bulk product consisting mainly of platelike crystals and starlike agglomerations of thin needles.
(14) A. Müller, W. Eltzner, W. Clegg, and G. M. Sheldrick, *Angew. Chem.*, **94**, 555 (1982); *Angew. Chem., Int. Ed. Engl.*, **21**, 536 (1982); *Angew. Chem. Suppl.*, 1177 (1982).
(15) A. Müller, R. G. Bhattacharyya, N. Mohan, and B. Pfefferkorn, *Z. Anorg. Allg. Chem.*, **454**, 118 (1979).
(16) A. Müller, W. Eltzner, E. Krickemeyer, and H. Bögge, manuscript in preparation. For the corresponding NH_4^+ salt see: A. Müller, W. O. Nolte, and B. Krebs, *Inorg. Chem.* **19**, 2835 (1980); A. Müller, R. G. Bhattacharyya, and B. Pfefferkorn, *Chem. Ber.*, **112**, 778 (1979).
(17) **2c** was characterized by an X-ray structure analysis: space group $Pa3$, a = 18.861 (5) Å, Z = 8, R = 0.074. The structure of the anion (d(Mo–Mo) = 2.767 (2) Å) is practically identical with that in **2b**; thus, no further details are given.
(18) A. Müller, W. Eltzner, H. Bögge, and S. Sarkar, *Angew. Chem.*, **94**, 555 (1982); *Angew. Chem., Int. Ed. Engl.* **21**, 535 (1982); *Angew. Chem. Suppl.*, 1167 (1982).

Table I. Summary of Crystal Data and Intensity Collection for $K_5[Mo_3S_4(CN)_9]\cdot 3KCN\cdot 4H_2O$ (**2b**) and $[(C_6H_5)_4P]_4[Mo_2S_2(CN)_8]\cdot nH_2O$ (**4b**)

	2b	**4b**
empirical formula	$C_{12}H_8K_8Mo_3N_{12}O_4S_4$	$C_{104}H_{80}Mo_2N_8P_4S_2\cdot nH_2O$
fw	1113.2	1821.8[a]
cryst dimens, mm	0.2 × 0.25 × 0.4	0.05 × 0.3 × 0.3
cryst syst	monoclinic	orthorhombic
space group	*Cm*	*Pnna*
a, Å	15.661 (3)	29.871 (21)
b, Å	18.807 (3)	24.278 (26)
c, Å	6.552 (1)	13.405 (11)
β, deg	116.39 (1)	
V, Å^3	1728.6	9721.5
Z	2	4
d_{calcd}, g/cm^3	2.14	1.24[a]
μ(Mo Kα), cm^{-1}	22.7	4.1[a]
F(000), electrons	1076	3744[a]
radiation[b]	Mo Kα (λ = 0.71069 Å)	Mo Kα (λ = 0.71069 Å)
scan mode	θ–2θ scan	ω scan
2θ range, deg	4–54	4–42
scan range	1° below Kα_1 to 1° above Kα_2 in 2θ	1° in ω bisected by K$\alpha_{1,2}$ max
scan speed, deg/min	2.9–29.3	2.7–29.3
bkgd/scan time ratio	0.75	0.8
ref reflcn	1 reflcn every 50 reflcns	1 reflcn every 39 reflcns
no. of measd reflcns	2042	5871
no. of indep reflcns ($F_o > 3.92\sigma(F_o)$)	1985	1868
no. of variables	191	156

[a] Calculated for $n = 0$. [b] Graphite monochromator.

Physical Measurements. IR spectra were recorded on a Perkin-Elmer instrument (Model 180) using CsI pellets or Nujol suspensions with CsBr or polyethylene windows. A 0.025-mm CaF_2 window was used for the measurements of the solutions.

Raman and resonance Raman spectra of the solid samples (rotating-cell technique) were obtained with a Spex Ramanlog 5 M or Coderg T 800 instrument equipped with a Coherent CR 4 (λ_e = 488.0 and 514.5 nm) or CR 500 K (λ_e = 647.1 nm) laser.

The near-IR/vis/UV spectra were recorded with the Acta M IV spectrophotometer of Beckman Inc. The stability of the complexes in solution was checked by comparing solution spectra and solid-state reflection spectra. Due to the very rapid decomposition of **3** in highly diluted aqueous solution, the spectrum of Figure 7 was obtained from several time-dependent measurements with extrapolation to $t = 0$.

X-ray photoelectron spectra were recorded with the ESCALAB 503 spectrometer of Vacuum Generators with the Al Kα line (1486.6 eV) as the excitation source. The spectra were calibrated with use of the C 1s binding energy (285.0 eV) from pump oil as internal standard.

The powder diffractogram of **1a** was obtained with a Philips PW 1050/70 instrument (Cu Kα radiation).

Cyclic voltammograms were measured using the CV 1A instrument of Bioanalytical Systems in connection with a Linseis x-y recorder (typical scan rate 100 mV/s). A three-electrode geometry was used with Pt electrodes as working and auxiliary electrodes (carbon-paste electrode as working electrode for measurements in aqueous solution); potentials were determined with an Ag/AgCl/3 M NaCl reference electrode (E_N = +0.2223 V). The concentrations of **3a** or **4a** were 10^{-3} M in 10^{-1} M solutions of KCl in H_2O (**3a**) or $[(C_2H_5)_4N][PF_6]$ in Me_2SO (**4a**).

X-ray Structure Determinations. The structures of $K_5[Mo_3S_4(CN)_9]\cdot 3KCN\cdot 4H_2O$ (**2b**) and $[(C_6H_5)_4P]_4[Mo_2S_2(CN)_8]\cdot nH_2O$ (**4b**) were determined from single-crystal data (Syntex $P2_1$ four-circle diffractometer). Summaries of the crystal data and details concerning the intensity data collection are given in Table I. The unit cell parameters were obtained at 21 °C by a least-squares refinement of the angular settings of high-angle reflections. An empirical absorption correction was applied for **2b**. The data were corrected for Lorentz and polarization effects.

The structures were solved by conventional heavy-atom methods (Syntex XTL and SHELX-76 program package for **2b** and **4b** respectively). After detection of the heavy atoms the positional parameters of the remaining non-hydrogen atoms were deduced from successive difference-Fourier syntheses. The final least-squares refinement converged at $R = \sum||F_o| - |F_c||/\sum|F_c| = 0.031$ (**2b**) and 0.157 (**4b**) and $R_w = (\sum w(|F_o| - |F_c|)^2/\sum w|F_o|^2)^{1/2} = 0.043$ (**2b**) and 0.147 (**4b**); $1/w = \sigma^2(F_o)$. During the last cycles of refinement no parameter shifted more than 0.1σ, where σ is the standard deviation of the parameter: Due to the small number of reflections, only Mo and S were refined anisotropically in **4b**.

The last difference Fourier synthesis for **4b** showed some minor peaks (<1.5 e/Å^3). These should be due to the water molecules, the positions of which could not be refined because of the bad data set.

The atomic scattering factors for all atoms were taken from standard sources.[19] Anomalous dispersion corrections were applied to all atoms. Positional parameters for **2b** and **4b** are given in Tables II and III, respectively. Lists of observed and calculated structure factors as well as thermal parameters are available (Tables SI–SIV of the supplementary material).

Table II. Positional Parameters for $K_5[Mo_3S_4(CN)_9]\cdot 3KCN\cdot 4H_2O$ with Standard Deviations

atom	*x*	*y*	*z*
Mo1	0.0	0.0	0.0
Mo2	−0.1612 (1)	0.0739 (1)	−0.2912 (1)
S1	−0.0711 (2)	0.0946 (1)	0.0939 (4)
S2	−0.2787 (2)	0.0	−0.2808 (6)
S3	−0.0679 (2)	0.0	−0.4031 (5)
C1	0.1038 (9)	0.0	0.3584 (21)
C2	0.1073 (6)	0.0743 (5)	−0.0127 (14)
C3	−0.0850 (6)	0.1625 (5)	−0.3647 (15)
C4	−0.2484 (7)	0.1634 (5)	−0.2763 (14)
C5	−0.2534 (7)	0.0931 (5)	0.3406 (16)
N1	0.1616 (9)	0.0	−0.4598 (21)
N2	0.1660 (6)	0.1112 (4)	−0.0092 (15)
N3	−0.0462 (6)	0.2092 (5)	−0.3927 (14)
N4	−0.2925 (6)	0.2109 (4)	−0.2683 (14)
N5	−0.3053 (6)	0.1035 (5)	0.1571 (15)
K1	0.1185 (2)	−0.1591 (1)	0.5323 (4)
K2	0.2756 (2)	0.2401 (1)	0.2056 (4)
K3	−0.4371 (3)	0.0	0.1864 (7)
K4	0.0388 (2)	0.3526 (1)	−0.2796 (4)
K5	0.3001 (2)	0.0	0.0101 (6)
C,N1[a]	0.4328 (9)	0.0	0.6196 (22)
C,N2[a]	−0.0596 (3)	0.3594 (2)	0.1379 (7)
O(H_2O)1	−0.1971 (6)	0.3543 (4)	−0.4408 (14)
O(H_2O)2	0.0867 (6)	0.2417 (4)	0.1420 (13)

[a] The individual C and N positions of the solvate CN^- ions could not be resolved.

Results and Discussion

In this section, first of all, details regarding the structures of the species under investigation are reported. Afterwards, a vibrational study of **1** (the complex with the highest symmetry) is described, which allows us to understand the basic principles of the coupling of the modes in the other species. The last part deals with spectroscopic data related to the electronic structures.

X-ray Structure Investigations. The molecular structures of the cyanothiomolybdates are given in Figure 1. Details of the structures of $K_8[Mo_4S_4(CN)_{12}]\cdot 4H_2O$ (**1a**),[6] $Ba_3[Mo_2S_2(CN)_8]\cdot 14H_2O$,[10] and $K_6[Mo_2S(CN)_{12}]\cdot 4H_2O$ (**5a**)[20] have been given elsewhere (some important results concerning that of $K_5[Mo_3S_4(CN)_9]\cdot 3KCN\cdot 4H_2O$ (**2b**) in a short paper[7]). The structure of $[(C_6H_5)_4P]_4[Mo_2S_2(CN)_8]\cdot nH_2O$ (**4b**) and details of the structure of **2b** are reported here for the first time.

(a) Single-Crystal Structure of $K_5[Mo_3S_4(CN)_9]\cdot 3KCN\cdot 4H_2O$ (2b) and $[(C_6H_5)_4P]_4[Mo_2S_2(CN)_8]\cdot nH_2O$ (4b). **2b** crystallizes in the monoclinic space group *Cm* ($Z = 2$). The structure contains discrete $[Mo_3S_4(CN)_9]^{5-}$ ions (**2**, see Figure 2) with the atoms Mo1, S2, S3, C1, and N1 lying on the mirror plane (x, 0, z). Thus, the crystallographic symmetry of **2** is C_s and the idealized symmetry C_{3v} (for bond distances and angles see Table IV). The central $\{Mo_3S_4\}$ unit represents an incomplete cube; **2** is formally a fragment of $[Mo_4S_4(CN)_{12}]^{8-}$ (**1**). The geometry of the $Mo_3(\mu_3\text{-}S)$ fragment is practically identical with that of the "parent cluster"[7] $[Mo_3S(S_2)_6]^{2-}$.[21] The average distance from the doubly

(19) "International Tables for X-ray Crystallography", Vol. IV, Kynoch Press, Birmingham, England, 1974.
(20) C. Potvin, J. M. Manoli, J. M. Brégeault, and G. Chottard, *Inorg. Chim. Acta*, **72**, 103 (1983).

Table III. Positional Parameters for $[(C_6H_5)_4P]_4[Mo_2S_2(CN)_8]\cdot nH_2O$ with Standard Deviations

atom	x	y	z
Mo	0.1391 (1)	0.1936 (2)	0.2381 (3)
S1	0.0778 (5)	0.25	0.25
S2	0.2007 (6)	0.25	0.25
CA1[a]	0.1326 (15)	0.1845 (19)	0.0863 (34)
N1	0.1294 (17)	0.1869 (22)	−0.0018 (42)
CA2	0.0925 (16)	0.1231 (20)	0.2208 (36)
N2	0.0696 (14)	0.0858 (19)	0.2186 (33)
CA3	0.1877 (17)	0.1310 (21)	0.2463 (49)
N3	0.2139 (14)	0.0939 (18)	0.2201 (33)
CA4	0.1408 (21)	0.1634 (22)	0.3858 (43)
N4	0.1440 (18)	0.1534 (20)	0.4707 (39)
P1	0.4472 (4)	0.3803 (5)	0.1475 (10)
P2	0.3297 (5)	0.3959 (6)	0.6872 (11)
C1[b]	0.4368 (12)	0.4365 (13)	0.0579 (25)
C2	0.4582 (12)	0.4378 (13)	−0.0345 (25)
C3	0.4503 (12)	0.4813 (13)	−0.1002 (25)
C4	0.4209 (12)	0.5234 (13)	−0.0735 (25)
C5	0.3995 (12)	0.5221 (13)	0.0189 (25)
C6	0.4074 (12)	0.4787 (13)	0.0846 (25)
C7	0.4848 (11)	0.4069 (14)	0.2460 (23)
C8	0.5173 (11)	0.3729 (14)	0.2883 (23)
C9	0.5417 (11)	0.3909 (14)	0.3709 (23)
C10	0.5335 (11)	0.4429 (14)	0.4112 (23)
C11	0.5010 (11)	0.4769 (14)	0.3689 (23)
C12	0.4766 (11)	0.4589 (14)	0.2863 (23)
C13	0.3950 (9)	0.3609 (13)	0.1979 (30)
C14	0.3558 (9)	0.3599 (13)	0.1414 (30)
C15	0.3158 (9)	0.3418 (13)	0.1842 (30)
C16	0.3151 (9)	0.3248 (13)	0.2836 (30)
C17	0.3543 (9)	0.3258 (13)	0.3401 (30)
C18	0.3942 (9)	0.3439 (13)	0.2973 (30)
C19	0.4794 (11)	0.3188 (11)	0.1005 (20)
C20	0.4536 (11)	0.2713 (11)	0.0900 (20)
C21	0.4681 (11)	0.2288 (11)	0.0279 (20)
C22	0.5084 (11)	0.2339 (11)	−0.0239 (20)
C23	0.5342 (11)	0.2814 (11)	−0.0135 (20)
C24	0.5197 (11)	0.3239 (11)	0.0487 (20)
C25	0.3854 (9)	0.3747 (14)	0.7104 (26)
C26	0.4223 (9)	0.3942 (14)	0.6571 (26)
C27	0.4652 (9)	0.3760 (14)	0.6811 (26)
C28	0.4713 (9)	0.3382 (14)	0.7582 (26)
C29	0.4345 (9)	0.3186 (14)	0.8115 (26)
C30	0.3915 (9)	0.3369 (14)	0.7875 (26)
C31	0.3037 (14)	0.3427 (18)	0.6138 (28)
C32	0.3167 (14)	0.2876 (18)	0.6200 (28)
C33	0.2929 (14)	0.2474 (18)	0.5679 (28)
C34	0.2561 (14)	0.2623 (18)	0.5095 (28)
C35	0.2432 (14)	0.3174 (18)	0.5033 (28)
C36	0.2670 (14)	0.3576 (18)	0.5555 (28)
C37	0.3010 (11)	0.4042 (13)	0.8005 (20)
C38	0.3192 (11)	0.4320 (13)	0.8819 (20)
C39	0.2940 (11)	0.4390 (13)	0.9687 (20)
C40	0.2506 (11)	0.4180 (13)	0.9740 (20)
C41	0.2324 (11)	0.3901 (13)	0.8926 (20)
C42	0.2576 (11)	0.3832 (13)	0.8058 (20)
C43	0.3355 (15)	0.4564 (18)	0.6139 (43)
C44	0.3340 (15)	0.5078 (18)	0.6603 (43)
C45	0.3413 (15)	0.5556 (18)	0.6046 (43)
C46	0.3500 (15)	0.5519 (18)	0.5026 (43)
C47	0.3515 (15)	0.5004 (18)	0.4563 (43)
C48	0.3443 (15)	0.4527 (18)	0.5119 (43)

[a] CA stands for C (anion). [b] The phenyl rings were refined as regular hexagons (C–C = 1.395 Å).

bridging sulfur atoms to the Mo atoms (2.322 Å) is slightly shorter than the average value of 2.361 Å for the distances from the triply bridging S atom. The average value of Mo–S–Mo angles subtended at the triply bridging sulfur atom is 71.9° and that subtended at the doubly bridging sulfur atoms 73.3°. The bond

(21) A. Müller, S. Pohl, M. Dartmann, J. P. Cohen, J. M. Bennett, and R. M. Kirchner, *Z. Naturforsch., B: Anorg. Chem., Org. Chem.*, **34B**, 434 (1979); E. Diemann, A. Müller, and P. J. Aymonino, *Z. Anorg. Allg. Chem.*, **479**, 191 (1981).

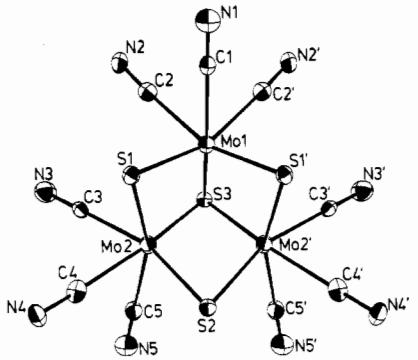

Figure 2. Structure of $[Mo_3S_4(CN)_9]^{5-}$ (ORTEP plot) in crystals of $K_5[Mo_3S_4(CN)_9]\cdot 3KCN\cdot 4H_2O$.

Table IV. Interatomic Distances (Å) and Angles (deg) for the Anion in $K_5[Mo_3S_4(CN)_9]\cdot 3KCN\cdot 4H_2O$ with Standard Deviations

Mo1–Mo2	2.769 (1)	Mo2–C3	2.222 (9)
Mo2–Mo2'[a]	2.781 (1)	Mo2–C4	2.196 (10)
		Mo2–C5	2.222 (10)
Mo1–S1	2.324 (2)		
Mo1–S3	2.368 (3)	C1–N1	1.131 (18)
Mo2–S1	2.312 (2)	C2–N2	1.144 (14)
Mo2–S2	2.331 (3)	C3–N3	1.129 (13)
Mo2–S3	2.358 (3)	C4–N4	1.145 (13)
Mo1–C1	2.182 (13)	C5–N5	1.130 (13)
Mo1–C2	2.216 (10)		
		S2–Mo2–C5	89.3 (3)
S1–Mo1–S1'	100.0 (1)	S3–Mo2–C3	84.7 (3)
S1–Mo1–S3	105.4 (1)	S3–Mo2–C4	161.6 (3)
S1–Mo1–C1	86.0 (3)	S3–Mo2–C5	87.2 (3)
S1–Mo1–C2	89.3 (2)	C3–Mo2–C4	80.8 (4)
S1–Mo1–C2'	162.6 (2)	C3–Mo2–C5	78.2 (4)
S3–Mo1–C1	161.9 (3)	C4–Mo2–C5	78.9 (4)
S3–Mo1–C2	86.0 (3)		
C1–Mo1–C2	80.0 (4)	Mo1–S1–Mo2	73.4 (1)
C2–Mo1–C2'	78.2 (3)	Mo2–S2–Mo2'	73.2 (1)
		Mo1–S3–Mo2	71.7 (1)
S1–Mo2–S2	100.1 (1)	Mo2–S3–Mo2'	72.3 (1)
S1–Mo2–S3	106.1 (1)		
S2–Mo2–S3	105.3 (1)	Mo1–C1–N1	176.1 (11)
S1–Mo2–C3	89.1 (3)	Mo1–C2–N2	176.5 (8)
S1–Mo2–C4	85.0 (3)	Mo2–C3–N3	176.5 (9)
S1–Mo2–C5	160.8 (3)	Mo2–C4–N4	178.7 (9)
S2–Mo2–C3	163.7 (3)	Mo2–C5–N5	175.3 (9)
S2–Mo2–C4	86.7 (3)		

[a] Symmetry transformation $x, \bar{y}, z$.

Table V. Interatomic Distances (Å) and Angles (deg) for the Anion in $[(C_6H_5)_4P]_4[Mo_2S_2(CN)_8]\cdot nH_2O$ with Standard Deviations

Mo–Mo	2.758 (7)	Mo–CA3	2.10 (5)
		Mo–CA4	2.11 (6)
Mo–S1	2.293 (13)		
Mo–S2	2.298 (14)	CA1–N1	1.19 (7)
		CA2–N2	1.14 (7)
Mo–CA1[a]	2.06 (5)	CA3–N3	1.24 (7)
Mo–CA2	2.22 (5)	CA4–N4	1.17 (8)
S1–Mo–S2	106.1 (4)	CA2–Mo–CA3	83 (2)
S1–Mo–CA1	93 (1)	CA2–Mo–CA4	81 (2)
S1–Mo–CA2	88 (1)	CA3–Mo–CA4	72 (2)
S1–Mo–CA3	168 (2)		
S1–Mo–CA4	99 (2)	Mo–S1–Mo'[b]	74.0 (5)
S2–Mo–CA1	102 (1)	Mo–S2–Mo'	73.8 (5)
S2–Mo–CA2	166 (1)		
S2–Mo–CA3	83 (1)	Mo–CA1–N1	171 (4)
S2–Mo–CA4	97 (2)	Mo–CA2–N2	175 (4)
		Mo–CA3–N3	160 (5)
CA1–Mo–CA2	76 (2)	Mo–CA4–N4	171 (5)
CA1–Mo–CA3	92 (2)		
CA1–Mo–CA4	153 (2)		

[a] CA stands for C (anion). [b] Symmetry transformation $x, 0.5 - y, 0.5 - z$.

Table VI. Average Distances and Intense Low-Frequency Raman Bands (Corresponding to Vibrations with Predominant ν_s(MoMo) Character)[d]

	av dist, Å					
	Mo–Mo	Mo–S	Mo–C	C–N	ref	"ν_s(MoMo)", cm^{-1}
$[Mo_4S_4(CN)_{12}]^{8-}$ (**1**)	2.855	2.381	2.191	1.138	6	228
$[Mo_3S_4(CN)_9]^{5-}$ (**2**)	2.773	2.322[a] 2.361[b]	2.210	1.136	this work	160
$[Mo_2S_2(CN)_8]^{6-}$ (**3**)	2.644	2.365	[e]	[e]	10	195
$[Mo_2S_2(CN)_8]^{4-}$ (**4**)	2.758	2.296	2.12	1.18	this work	185
$[Mo_2S(CN)_{12}]^{6-}$ (**5**)	...	2.172	2.172	1.146	18	...
$[Mo_4S_4(NO)_4(CN)_8]^{8-}$	2.99	2.35[c]	2.21	1.16	13	177
$[Mo_2S_2(NO)_2(CN)_6]^{6-}$						175
$K_4[Mo(CN)_8]\cdot 2H_2O$	...	...	2.163	1.152	20	

[a] d(Mo–(μ-S)). [b] d(Mo–(μ_3-S)). [c] d(Mo–S) (cis NO). [d] For the type of salt see the Experimental Section; λ_e = 647.1 nm. [e] Not reported.

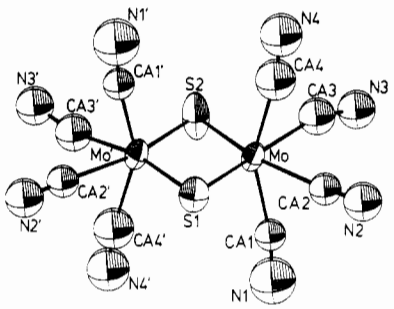

Figure 3. Structure of $[Mo_2S_2(CN)_8]^{4-}$ (ORTEP plot) in crystals of $[(C_6H_5)_4P]_4[Mo_2S_2(CN)_8]\cdot nH_2O$.

distances within the nearly linear MoCN moieties (d_{av}(Mo–C) = 2.210 Å, d_{av}(C–N) = 1.136 Å) are of the expected order.[22]

4b crystallizes in the orthorhombic space group *Pnna* with four formula units per unit cell (lattice constants and space group suggest that the compound is isostructural with $[(C_6H_5)_4P]_4[Re_2S_2(CN)_8]\cdot 6H_2O$[23]); the two sulfur atoms of the anion **4** are lying on the twofold axis (x, $^1/_4$, $^1/_4$). Thus, the crystallographic symmetry of **4** is C_2 and the idealized symmetry D_{2h} (for bond distances and angles see Table V). The anion (see Figure 3) contains planar $Mo(S_{br})_2Mo$ units (d(Mo–Mo) = 2.758 (7) Å, d_{av}(Mo–S) = 2.296 Å) with pseudooctahedral coordination of the Mo atoms (two bridging S atoms and four cyano ligands; d_{av}(Mo–C) = 2.12 Å, d_{av}(C–N) = 1.18 Å). The Mo–Mo bond in **4** is significantly longer than in $[Mo_2S_2(CN)_8]^{6-}$ (**3**, 2.644 Å), while the Mo–S bonds are shorter (**3**, 2.365 Å;[10] for discussion see Electronic Structure and Spectra). Chemical analysis of the bulk product suggests a water content of n = 2; however, due to the poor quality of the data set, it cannot be excluded that the single crystal used for the structure determination had a different water content.

Averaged structural data of the cyanothiomolybdates and some related complexes are summarized in Table VI. The values show that the Mo–Mo interaction is strongest in **3** and the Mo–S interaction strongest in **4** and **5**. A high Mo–C bond order can typically be correlated with a weakening of the C–N bonds (further discussion below).

(b) Powder Diffraction Data of $K_8[Mo_4S_4(CN)_{12}]\cdot 4H_2O$ (1a). **1a** has been studied by both single-crystal[6] and powder diffraction techniques. It crystallizes in a tetragonal unit cell with a = 12.361 (5) Å and c = 11.363 (5) Å and two formula units. The space group is $P4_2/nmc$. Here we report the powder diffraction data (Table VII), since due to the high symmetry of **1a** the diffractogram shows only a few lines, which can be indexed and thus serve to identify the substance. It is interesting to note that the powder diffraction diagram is practically identical with that of $K_8[Mo_4S_4(NO)_4(CN)_8]\cdot 4H_2O$.[14]

Vibrational Study of $[Mo_4S_4(CN)_{12}]^{8-}$: Symmetry Coordinates for an $M_4X_4(YZ)_{12}$ Type Species with a Distorted M_4X_4 Cube and

Table VII. Powder Diffraction Data for $K_8[Mo_4S_4(CN)_{12}]\cdot 4H_2O$[c]

$2\theta_{obsd}$, deg[a]	$2\theta_{calcd}$, deg	d_{obsd}, Å	hkl	I_{rel}[b]
10.18	10.12	8.69	110	st
10.45	10.44	8.47	101	m
14.35	14.33	6.17	200	m
17.76	17.76	4.99	211	m
18.33	18.32	4.84	112	w
20.38	20.32	4.36	220	m
22.20	22.18	4.00	212	m
22.75	22.75	3.91	310	w
26.53	26.51	3.36	302	m
28.90	28.89	3.09	400	w
30.69	30.69/30.73	2.91	330/004	vst
32.40	32.39	2.76	420	m
33.35	33.32	2.69	421	m
37.15	37.18	2.42	431	m
37.90	37.86/37.91	2.37	304/511	m
39.60	39.61	2.28	502	m
40.05	40.06	2.25	423	m
41.33	41.32	2.18	440	m
42.66	42.65	2.12	530	m
43.34	43.34	2.09	414	m
43.96	43.95/43.98	2.06	600/334	m
45.72	45.54	1.98	532	m
48.90	48.91/48.97	1.86	514/533	w
52.32	52.33/52.37	1.75	550/444	m

[a] Cu Kα radiation. [b] Relative intensity: vst = very strong, st = strong, m = medium, w = weak. [c] Complete single-crystal structure analysis in *Angew. Chem. Suppl.*[6]

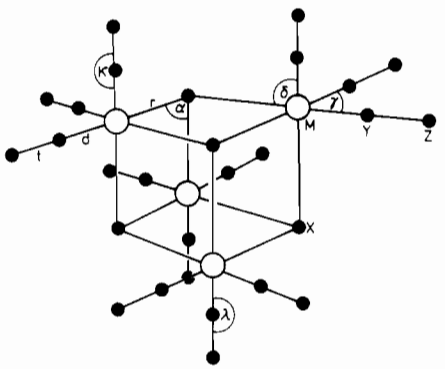

Figure 4. The $M_xX_x(YZ)_{12}$ model with indication of some representative valence coordinates.

Linear MYZ Groups (T_d Symmetry). According to the X-ray structure analysis $[Mo_4S_4(CN)_{12}]^{8-}$ (**1**) has practically T_d symmetry.[6] A normal-coordinate treatment and detailed vibrational analysis for this type of species has not been reported until now. In spite of the high symmetry of **1** the assignment of the IR and Raman spectra is not so easy according to the large number of vibrational degrees of freedom ($3N - 6 = 90$).

The symmetry coordinates derived for a molecular model of $(TeCl_4)_4$[24] are applicable to the species **1** when the CN groups

(22) J. L. Hoard, T. A. Hamor, and M. D. Glick, *J. Am. Chem. Soc.*, **90**, 3177 (1968).
(23) M. Laing, J. M. Brégeault, and W. P. Griffith, *Inorg. Chim. Acta*, **26**, L27 (1978).
(24) S. J. Cyvin, B. N. Cyvin, W. Brockner, and A. F. Demiray, *Z. Naturforsch., A*, **33A**, 714 (1978).

Table VIII. Types of Valence Coordinates Used for the Construction of a Set of Independent Symmetry Coordinates for the $M_4X_4(YZ)_{12}$ Model with Symmetry T_d[a]

	$6A_1$	$2A_2$	8E	$9T_1$	$13T_2$
M_4X_4 cube	r		r	r	r
					r
	α		α		α
$M(YZ)_3$	d		d	d	d
					d
	γ		γ	γ	γ
					γ
	t		t	t	t
					t
	κ		κ	κ	κ
					κ
		λ	λ	λ	λ
				λ	
coupling part		δ	δ	δ	δ
				δ	

[a] An alternative choice of coordinates does not influence the calculations.

(YZ) are considered as point masses. The analysis was extended to the complete species **1** by including the YZ stretching and MYZ linear bendings. The $M_4X_4(YZ)_{12}$ model is depicted in Figure 4 with the indication of some representative valence coordinates. The normal modes of vibrations are distributed among the symmetry species of the T_d group according to

$$\Gamma_{vib} = 6A_1(R) + 2A_2 + 8E(R) + 9T_1 + 13T_2(IR,R)$$

A complete set of independent symmetry coordinates was deduced; Table VIII shows the types of valence coordinates used for this purpose. The designations are explained in the following, where the multiplicity of each type is shown in parentheses: d = MY stretching (12); γ = YMY bending (12); r = MX stretching (12); α = MXM bending (12); δ = XMY bending (24); t = YZ stretching (12); κ = MYZ linear bending in a plane through the model center (12); λ = MYZ linear bending in a plane perpendicular to the one through the model center (12).

Notice that there are 24 δ-type bendings (see above) but only 12 combinations were used in the construction of the symmetry coordinates (cf. Table VIII). The rest of them are present as redundancies, since all δ bendings were included in the basis of the force field. In a similar way only 6 combinations of the 12 α bendings are used in the symmetry coordinates. The actual symmetry-adapted linear combinations are given in the cited work.[24] One only has to add the following features concerning the extension with linear chains. The t- and κ-type coordinates follow the pattern of most of the other types, which have been represented by the symbol q in ref 24. The λ-type linear bendings transform like the differences of δ-type bendings identified with the symbol τ in ref 24.

The assumed force-field approximation is defined by a diagonal force-constant matrix in terms of valence coordinates including redundancies. It should be mentioned that the arbitrary removal of redundancies under the construction of symmetry coordinates does not affect the computed frequencies.[25] No force constant value was assigned explicitly to the S–Mo–S bendings; these motions are supposed to be sufficiently covered by the other coordinates of the cube. The six M–M stretchings were included in the basis of the force field (but the corresponding symmetry coordinates were not used, they were described in terms of α-(MXM)). The numerical values of the force constants are shown in Table IX and those of the calculated frequencies in Table X.

In spite of the *extremely* simple force field used in the analysis, neglecting *all* (!) interaction force constants, the calculated frequencies (Table X) at least for the Mo_4S_4 cube are in reasonable agreement with the measured spectra (see below), thus allowing

(25) S. J. Cyvin, B. N. Cyvin, M. Somer, and W. Brockner, *Z. Naturforsch., A*, **36A**, 774 (1981).

Table IX. Final Force Constants (mdyn/Å) of **1** Used in the Calculation

stretchings	C–N	16.5
	Mo–C	2.2
	Mo–S	1.3
	Mo–Mo[a]	1.0
linear bendings	Mo–C–N	0.2
nonlinear bendings	C–Mo–C	0.2
	C–Mo–S	0.2
	Mo–S–Mo	0.1
	S–Mo–S[a]	0.0

[a] Not used in symmetry coordinates.

a satisfactory assignment (which is facilitated by the calculation of theoretical $^{92/100}$Mo and $^{32/34}$S isotope shifts). Due to the simple force field, the A_1-, E-, T_1-, and T_2-type ν(CN) vibrations were calculated to have identical frequencies (a consequence of the neglect of stretch/stretch interaction force constants). The agreement between the observed and calculated ν(MoC) and δ(MoCN) vibrations was not expected to be good as they are strongly coupled. The rather poor agreement for the two E-type ν(MoS) vibrations results from the same reason.

The measured vibrational frequencies are summarized in Table XI. The bands in the region of the ν(CN) vibrations (~2100 cm^{-1}) are easy to locate. It seems to be possible to distinguish between the M–S stretching vibrations (<370 cm^{-1}) on the one hand and the vibrations of the Mo–C–N linkage on the other hand (Mo–C stretchings and δ(MoCN) bendings (>370 cm^{-1}), which are strongly coupled).

A more detailed assignment is obtained with the help of the results of our normal-coordinate analysis (Table X), the selection rules, and the band intensities (A_1 fundamentals are the strongest bands in the Raman and T_2 bands the strongest bands in the IR).

The most interesting vibrations are those of the Mo_4S_4 cube (Table XII), which can be classified according to the species

$$\nu(MoS): \quad A_1 + E + T_1 + 2T_2$$

$$\nu(MoMo): \quad A_1 + E + T_2$$

(a) ν(MoMo). Whereas the E- and especially the A_1-type vibrations (Raman band at 228 cm^{-1}) can be considered to be rather characteristic (see Table X), the T_2 fundamental contains strong ν(MoS) contributions. The strong A_1 line in the Raman spectrum can be regarded as an analytical tool for the Mo_4S_4 cube.

(b) ν(MoS). The A_1 and T_2 fundamentals (Table XII) can be assigned straightforwardly (A_1, strong band in the Raman spectrum; T_2, strong band in the IR spectrum). These bands can also be considered to be highly characteristic for an $\{Mo_4S_4\}$ cube, especially because, according to the normal-coordinate analysis, practically only the S atoms move vs. the $\{Mo_4\}$ cluster system. This is also a nice indication for the existence of metal–metal interaction.

Some Other Aspects of the IR, Raman, and Resonance Raman Spectra of the Cyanothiomolybdates. Some results of IR and Raman spectra of complexes **1–5** lead to interesting conclusions concerning the chemical bonding.

(a) Frequencies and Intensities of ν(CN) Bands in the IR Spectra. The measurements of intensities of the ν(CN) infrared bands in solution is of special interest. The integrated absorption coefficient k[26] has been calculated from the molar extinction coefficient ϵ_m (measured at the absorption maximum of the strong ν(CN) band) and half-width under the assumption of a Lorentz function band shape (the much less intense bands of **1** and **5** do not add much to the total absorption and are, therefore, neglected). We discuss, however, the integrated absorption coefficient per CN^- ligand k_{CN} (obtained from k by simple division).

The ν(CN) frequencies and the molar extinction coefficients are listed in Table XIII. The frequencies are dependent on the oxidation state of molybdenum. Those of Mo^{III} are generally lower

(26) L. H. Jones, *Inorg. Chem.*, **2**, 777 (1963).

Table X. Calculated Vibrational Frequencies of **1** (cm^{-1}) and Assignments

species	point-mass (CN) model $[^{92}Mo_4{}^{32}S_4(CN)_{12}]^{8-}$	complete anion $[^{92}Mo_4{}^{32}S_4(CN)_{12}]^{8-}$	complete anion $[^{100}Mo_4{}^{32}S_4(CN)_{12}]^{8-}$	complete anion $[^{92}Mo_4{}^{34}S_4(CN)_{12}]^{8-}$	assignt[a]
A_1		2123	2123	2123	ν(CN)
	495	527	520	527	ν(MoC)
		447	444	447	δ(MoCN)
	380	373	373	363	ν(MoS)
	260	246	241	246	ν(MoMo)
	186	118	118	118	δ(CMoC)
A_2		433	433	433	δ'(MoCN)
	133	88	88	88	δ(CMoS)
E		2123	2123	2123	ν(CN)
	447	495	492	495	ν(MoC)
		455	452	455	δ(MoCN)
	285	407	405	406	δ'(MoCN)
	235	281	280	274	ν(MoS)
	190	193	189	192	ν(MoMo)
		119	119	119	δ(CMoC)
	61	47	47	47	δ(CMoS)
T_1		2123	2123	2123	ν(CN)
	441	492	490	492	ν(MoC)
		453	449	452	δ(MoCN)
		436	436	436	δ'(MoCN)
		404	403	404	δ'(MoCN)
	296	287	286	281	ν(MoS)
	224	151	149	150	δ(CMoC)
	167	113	113	113	δ(CMoS)
	123	83	83	83	δ(CMoS)
T_2		2123	2123	2123	ν(CN)
		2123	2123	2123	ν(CN)
	485	521	514	519	ν(MoC)
	461	503.1	500	502.7	ν(MoC)
		466	464	465	δ(MoCN)
		437.4	434	437.1	δ(MoCN)
		404	402.8	403.4	δ'(MoCN)
	380	369	369	363	ν(MoS)
	290	282	281	275	ν(MoS)
	227	186.2	182	185.5	ν(MoMo)
	195	124.5	124.0	124.4	δ(CMoC)
	175	118	118	118	δ(CMoC)
	107	75	75	75	δ(CMoS)

[a] δ refers to the linear bendings of the κ type and δ' to λ type; for assignment of δ(MoCN) and ν(MoC) see the text.

Table XI. IR and Raman Spectra of $K_8[Mo_4S_4(CN)_{12}]\cdot 4H_2O$ and Tentative Assignments[a]

IR freq, cm^{-1}	Raman freq, cm^{-1}	Raman rel intens[d]	tentative assignt
~145 m, br[b]			
~180 m, br			ν(MoMo), T_2
...	192	4.6	ν(MoMo), E
...	228[c]		ν(MoMo), A_1
313 m	316	0.8	ν(MoS), T_2
341 vs			ν(MoS), T_2
...	363	4.9	ν(MoS), E
...	372	10.0	ν(MoS), A_1
375 m			δ(MoCN), T_2
...	392	4.7	δ(MoCN), A_1
...	410	5.8	δ(MoCN), ν(MoC), E
417 m			δ(MoCN), ν(MoC), T_2
434 w	433	3.7	ν(MoC), T_2
...	448	2.8	ν(MoC), A_1
~550 m, br			H_2O libration
1624 m			$\delta(H_2O)$
2093 vs	2093	6.8	ν(CN), T_2
...	2100	7.6	ν(CN), A_1
~2113 w, sh	2112	2.1	ν(CN) T_2
...	2122	0.6	ν(CN), E
3490 s			$\nu(H_2O)$
3570 s			

[a] A reasonable Raman spectrum of the solution could not be obtained. [b] From polyethylene disk. [c] This band is overlapped by a plasma line. [d] λ_e = 647.1 nm.

Table XII. Vibrations of the Mo_4S_4 Core (cm^{-1}) of **1**

		calcd[a]	"obsd"
A_1	ν(MoS)	373	372
	ν(MoMo)	246	228
E	ν(MoS)	281	363
	ν(MoMo)	193	192
T_1	ν(MoS)	287	
T_2	ν(MoS)	369	341
	ν(MoS)	282	313
	ν(MoMo)	186	~180

[a] For $[^{92}Mo_4{}^{32}S_4(CN)_{12}]^{8-}$.

than those of Mo^{IV} complexes by approximately 30 cm^{-1}. The band intensities, however, are affected by the oxidation state of Mo in comparable complexes in a much more pronounced way.

The correlation between the oxidation state and the ν(CN) frequencies and their band intensities can be explained by the concept of σ donation and M→π^*(CN) back-bonding (see valence structures I and II).[26-28] The intensity is a measure of the degree

I II

of M–C π bonding, i.e., of the increasing importance of valence structure II. With an increasing number of (formal) Mo 4d electrons, the valence structure II gains more importance.

(27) W. P. Griffith and G. T. Turner, *J. Chem. Soc.* A, 858 (1970).
(28) K. Nakamoto, "Infrared and Raman Spectra of Inorganic and Coordination Compounds", 3rd ed., Wiley, New York, 1978.

Table XIII. ν(CN) Bands: Frequencies (cm^{-1}) and Intensities[a]

	oxidn state of Mo (electron confign)	ν(CN) solid	ν(CN) H_2O soln	ϵ_m in H_2O	k	k_{CN}
$K_8[Mo_4S_4(CN)_{12}]\cdot 4H_2O$ (**1a**)	Mo^{3+} $(d^3)_4$	2093 s 2113 w, sh	2087 s 2109 w	7480	141.0	12.0
$K_6[Mo_2S_2(CN)_8]\cdot 4H_2O$ (**3a**)	Mo^{3+} $(d^3)_2$	2084 s 2071 s 2058 w	2096 s	2060[b]	60.9	7.6[b]
$[(C_6H_5)_4P]_4[Mo_2S_2(CN)_8]\cdot 2H_2O$ (**4a**)	Mo^{4+} $(d^2)_2$	2114 s (2059 w?)	2120 s[c]	490[c]	14.2	1.8
$K_5[Mo_3S_4(CN)_9]\cdot 2H_2O$ (**2a**)	Mo^{4+} $(d^2)_3$	2122 s 2118 sh	2126 s	1520	38.3	4.3
$K_6[Mo_2S(CN)_{12}]\cdot 4H_2O$ (**5a**)	Mo^{4+} $(d^2)_2$	2132 s 2122 s 2118 s 2110 s	2121 s 2109 m	4370	74.2	6.2
$K_6[Mo_2S_2(NO)_2(CN)_6]\cdot 4H_2O$ (**6a**)	$\{MoNO\}^{2+}$	2095 s	2098 s	1570	39.6	6.6
$K_8[Mo_4S_4(NO)_4(CN)_8]\cdot 4H_2O$	$\{MoNO\}^{2+}$	2094 s	2092 s	3680	81.1	10.1

[a] ϵ_m = molar extinction coefficient (M^{-1} cm^{-1}); k = integrated absorption coefficient (10^3 M^{-1} cm^{-2}); k_{CN} = integrated absorption coefficient per CN^- ligand (10^3 M^{-1} cm^{-2}); estimated accuracy ±10%. [b] Approximate value because of decomposition in aqueous solution. [c] In CH_3OH solution.

Table XIV. Electronic Absorption Spectra of Cyanothiomolybdates: Frequencies (10^3 cm^{-1}) and ϵ Values (M^{-1} cm^{-1}) in Parentheses[a,b]

$[Mo_4S_4(CN)_{12}]^{8-}$ (**1**)	$[Mo_3S_4(CN)_9]^{5-}$ (**2**)	$[Mo_2S_2(CN)_8]^{6-}$ (**3**)	$[Mo_2S_2(CN)_8]^{4-}$ (**4**)	$[Mo_2S(CN)_{12}]^{6-}$ (**5**)
8.9 (150)	16.4 (500)	9.8 (820)	15.2 (3100)	16.1 (120)
15.2 (580)	26.5 (5500)	16.2 (1600)	31.2 (5200)	27.0 (64 000)
20.0 (sh)	29.2 (4500)	23.8 (sh)		33.3 (sh)
25.2 (sh)	35.7 (sh)	27.0 (sh)		38.5 (sh)
31.7 (14 300)	40.5 (17 000)	31.2 (sh)		42.0 (7700)
37.0 (32 000)	47.4 (23 000)	40.0 (sh)		43.1 (sh)
45.5 (24 500)		44.4 (12 000)		

[a] Estimated accuracy of the ϵ values ±5%. [b] Solvents as given in the legends to the corresponding figures.

Therefore, the intensity per CN^- ligand is higher in **3** (Mo^{III}) than in the almost isostructural **4** (Mo^{IV}), but also higher in **1** (Mo^{III}) than in **2** (Mo^{IV}), both having a comparable coordination of Mo, which means $\{Mo(CN)_3\}$ moieties linked by Mo–Mo single bonds (cf. Figures 1 and 2). The latter comparison is, of course, very rough since the vibrations involved are not of the same species. But our simple concept works and is justified by the first example. In this context it is remarkable (and a further justification for the simple treatment) that the two pseudoisostructural pairs **1** and $[Mo_4S_4(NO)_4(CN)_8]^{8-}$[14] as well as **3** and $[Mo_2S_2(NO)_2(CN)_6]^{6-}$ (**6**) have comparable values. This can be understood if the two nitrosyl complexes are considered as Mo^{III} complexes, leading to a *formal* description of NO^- for the nitrosyl ligands (which seems to be justified[29]).

The different influence of μ-S^{2-} and μ_3-S^{2-} ligands should be important, too. While μ-S^{2-} ligands typically carry a high negative charge, μ_3-S^{2-} ligands and the S atom of **5** are significantly less negative (see below). A higher value of k_{CN} in a tetranuclear system compared to that of the comparable dinuclear species is correspondingly found in the pair **6** and $[Mo_4S_4(NO)_4(CN)_8]^{8-}$. A similar effect (see results of MO calculations) is responsible for the high k_{CN} value of **5** (in comparison to those for the other Mo^{IV} systems).

(b) The Strong Low-Frequency Raman Bands Corresponding to Vibrations with Predominant ν(Mo–Mo) Character. With the exception of **5** the Mo atoms of all mentioned species are linked by metal–metal bonds of various strength. Each of the complexes shows at least one rather strong Raman band in the 150–230-cm^{-1} region (see Table VI). We know that in the case of **1** the corresponding band has to be assigned to a ν_s(MoMo) type vibration. Though the contribution of the metal–metal stretching coordinate is smaller for the other complexes, it is evident that the strong Raman bands mentioned here can be regarded as analytical tools for systems with Mo–Mo bonds and S^{2-} bridging ligands.

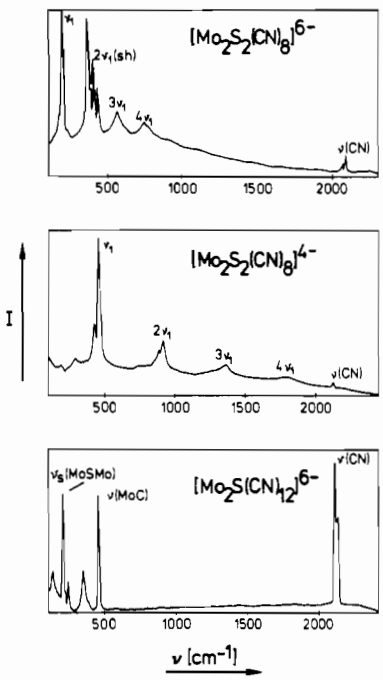

Figure 5. Resonance Raman spectra of $K_6[Mo_2S_2(CN)_8]\cdot 4H_2O$ (**3a**), $[(C_6H_5)_4P]_4[Mo_2S_2(CN)_8]\cdot 2H_2O$ (**4a**), and $K_6[Mo_2S(CN)_{12}]\cdot 4H_2O$ (**5a**). (λ_e = 647.1 nm.)

(c) Resonance Raman Studies. With use of the 647.1-nm line of a Kr^+ laser, good resonance Raman spectra of **2**, **3**, **4**, and **5** were obtained (see Figure 5), all of which have intense absorption maxima very near this wavelength (cf. Table XIV).

$[Mo_2S_2(CN)_8]^{4-}$ (**4**) and $[Mo_2S_2(CN)_8]^{6-}$ (**3**) show a strong enhancement of the 459- and 195-cm^{-1} bands, respectively (and progressions of the corresponding bands up to 4ν). It is reasonable

(29) This seems to be justified according to the extremely low ν(NO) frequencies (ca. 1450 cm^{-1}) for both complexes; see also B. Folkesson, *Acta Chem. Scand., Ser. A*, **A28**, 491 (1974).

Table XV. Results from the MO Calculations

	$[Mo_4S_4(CN)_{12}]^{8-}$	$[Mo_3S_4(CN)_9]^{5-}$	$[Mo_2S_2(CN)_8]^{6-}$	$[Mo_2S_2(CN)_8]^{4-}$	$[Mo_2S(CN)_{12}]^{6-}$
q(Mo)	0.100	0.126	0.048	0.130	0.115
q(S)	−0.048	−0.020[a]	−0.167	−0.034	0.091
		−0.070[b]			
Δq(CN)[c]	0.210	0.194	0.189	0.196	0.340
p(Mo–Mo)[d]	0.131	0.162	0.361	0.245	...
p(Mo–S)[d]	0.442	0.457[a]	0.492	0.609	0.972
		0.611[b]			
p(Mo–C)[d]	0.541	0.505	0.540	0.512	0.468
p(C–N)[d]	1.865	1.908	1.842	1.898	1.890

[a] μ_3-S. [b] μ-S. [c] Charge difference between C and N atoms, averaged if necessary. [d] Overlap population, averaged if necessary.

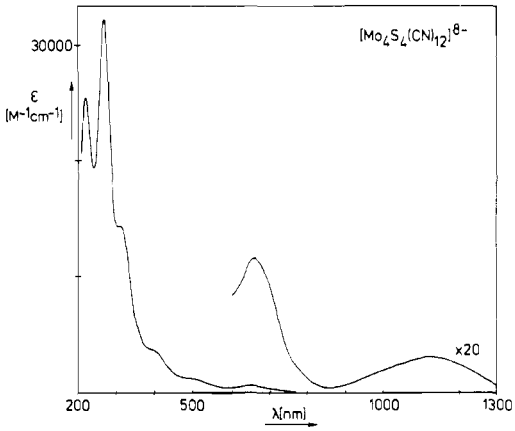

Figure 6. Electronic absorption spectrum of $[Mo_4S_4(CN)_{12}]^{8-}$ in H_2O (for the type of salts, used for the measurements of the spectra, see Experimental Section).

to assume that the 195-cm^{-1} line in **3** has to be assigned to a vibration of the type

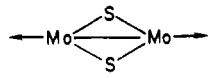

with predominant ν(MoMo) character, while the electronic absorption band at 16.2×10^3 cm^{-1} should be due to a transition within the metal–metal bonding system. According to the above-mentioned observation the 459-cm^{-1} band of **4** can be assigned to the vibration

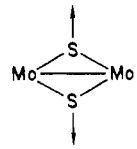

(indication of strong Mo–S π bonding because of the relatively high frequency, which is in agreement with the planarity of the MoS_2Mo system and the short MoS distance) and the affected electronic transition should have S 3p → π (Mo–Mo) charge-transfer character (see below).

A remarkable resonance Raman spectrum is obtained for $[Mo_2S(CN)_{12}]^{6-}$, the strongest bands being those for the symmetric vibrations of the MoSMo, MoC, and CN linkages (see Figure 5). This is a nice proof for delocalized orbitals over the whole complex (mainly over the linear NCMoSMoCN part).

The ν(MoMo) band in the Raman spectrum (λ_e = 514.5 nm) of $[Mo_3S_4(CN)_9]^{5-}$ at 160 cm^{-1} shows an enhanced intensity in the resonance Raman spectrum (λ_e = 647.1 nm), suggesting that the absorption at 16.4×10^3 cm^{-1} is caused by an electronic transition in the metal–metal bonding system (see below).

Electronic Structure and Spectra. In order to understand the electronic structures of the cyanothiomolybdates and to assign their electronic absorption spectra (presented in Table XIV and Figures 6–8), SCCC–EH–MO calculations have been made for all complexes (for computational details see Appendix). Some specific results, which allow a comparison of the electronic structures, are presented in Table XV. The bonding properties

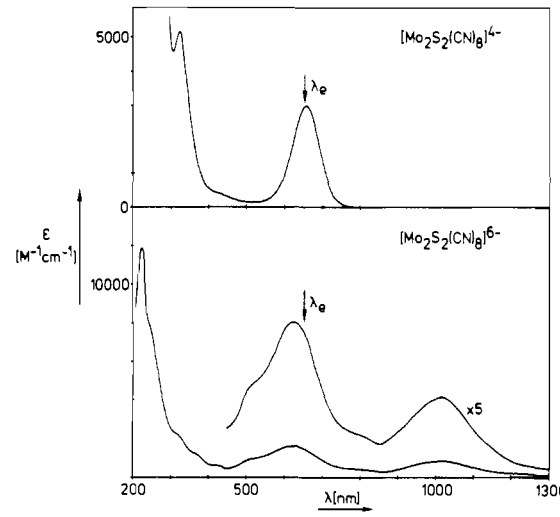

Figure 7. Electronic absorption spectra of $[Mo_2S_2(CN)_8]^{4-}$ (**4**) in DMF (above) and $[Mo_2S_2(CN)_8]^{6-}$ (**3**) in H_2O (below). The shoulders at 500 and 800 nm in the spectrum of **3** appear to be due to decomposition products.

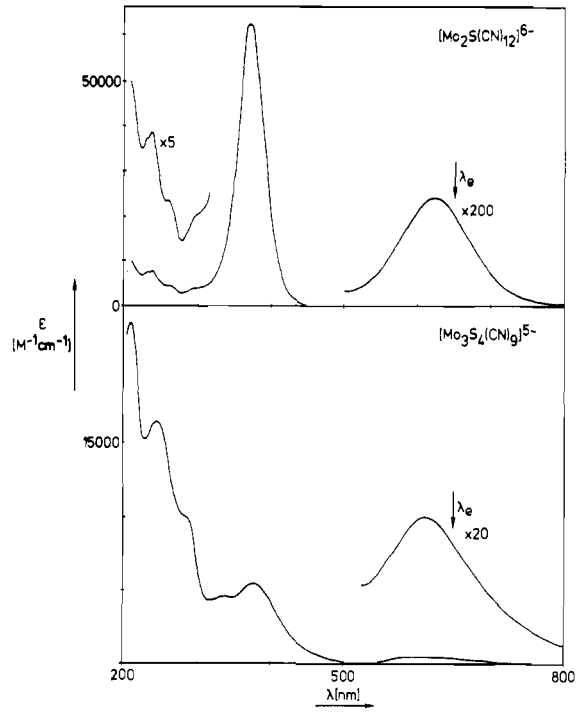

Figure 8. Electronic absorption spectra of $[Mo_2S(CN)_{12}]^{6-}$ (above) and $[Mo_3S_4(CN)_9]^{5-}$ (below) in H_2O.

have been studied especially with regard to the bonding within the Mo_xS_y cores.

The calculations show a common feature for all complexes: MOs, which are responsible for the bonding within the central Mo_xS_y moieties, are rather localized (~70–80% Mo 4d and S 3p).

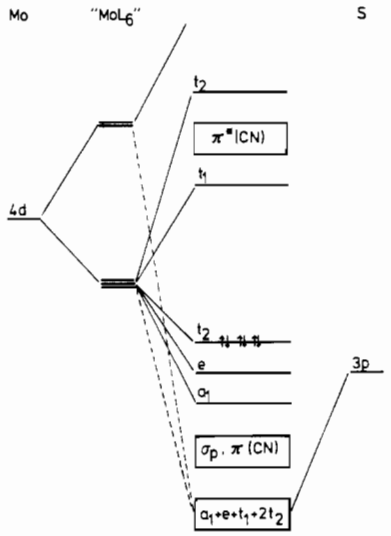

Figure 9. Qualitative MO scheme of $[Mo_4S_4(CN)_{12}]^{8-}$.

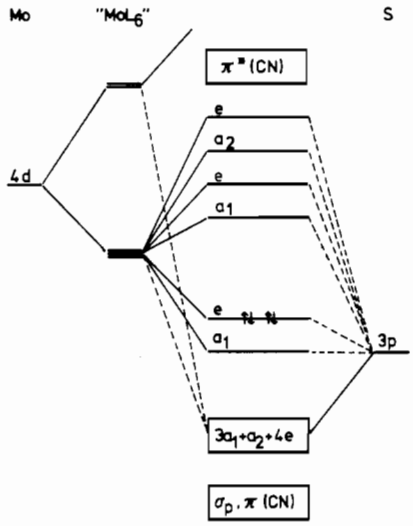

Figure 10. Qualitative MO scheme of $[Mo_3S_4(CN)_9]^{5-}$.

The HOMO/LUMO regions of all complexes are mainly determined by orbitals of this kind. The lower energy transitions ($\tilde{\nu} < 35 \times 10^3$ cm^{-1}) thus mainly take place within the Mo_xS_y chromophores.

Absorptions around 40×10^3 cm^{-1} (with ϵ values of ca. 10^4 M^{-1} cm^{-1}) in all complexes (just like in "pure" cyanomolybdates) have to be assigned to CN → Mo charge-transfer transitions.[30]

As the Mo–S and Mo–Mo interactions are the most interesting features of the electronic structures, we mainly discuss the MOs with predominant Mo and S character. These are presented in the MO schemes of Figures 9–12 (the HOMOs are indicated by arrows). The correlation lines designate major (—) and minor (- - -) contributions.

The results for the CN^- ligands are in agreement with the experimental vibrational data: the overlap populations reflect the variation of the ν(CN) frequencies, and the average charge differences between C and N atoms reflect the trends of the IR band intensities discussed above.

(a) $[Mo_4S_4(CN)_{12}]^{8-}$ (1). The calculation shows that our simple cluster model[31] can also be used to describe metal–metal bonding in tetranuclear clusters. In the HOMO/LUMO region there are six bonding (a_1, e, t_2; occupied in the complex) and six antibonding MOs (t_1, t_2; unoccupied), which have mainly Mo 4d character (this also explains the diamagnetism). Reversible electrochemical oxidation (see below) is facilitated by the only weak-bonding character of the occupied t_2 MO.

The cluster is mainly stabilized by the Mo–S bonding system (a_1, e, t_1, $2t_2$), which is formed predominantly from S 3p and Mo 4d AOs. The MO scheme (Figure 9) is somewhat similar to that derived for the tetranuclear electron-rich clusters of Fe and Co,[32] except for the fact that there are less low-lying metal-localized

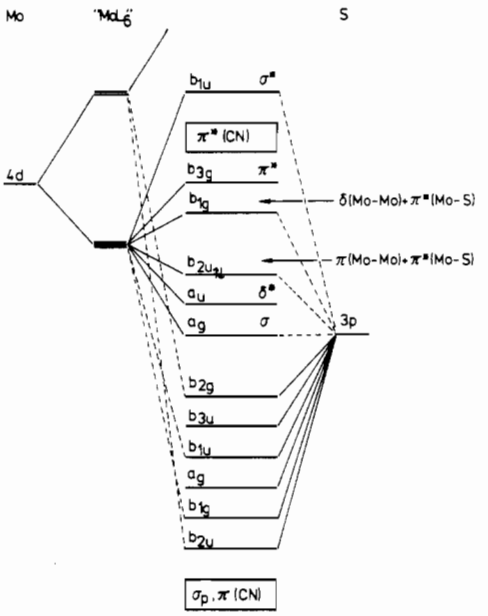

Figure 11. Qualitative MO scheme of $[Mo_2S_2(CN)_8]^{n-}$ (n = 4 (**4**), 6 (**3**)). $a_u(\delta^*)$ is the HOMO for **4**.

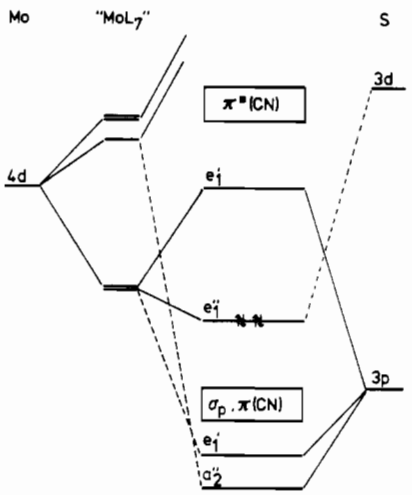

Figure 12. Qualitative MO scheme of $[Mo_2S(CN)_{12}]^{6-}$.

Table XVI. Sulfur 2p and Molybdenum $3d_{5/2}$ Electron Binding Energies for Some MoS Complexes (Values Relative to E_b(C1s) = 285.0 eV)

compd	oxidn state of Mo	type of Mo–S bond[a]	E_b, eV S 2p	E_b, eV Mo $3d_{5/2}$
$[(C_6H_5)_4P]_2MoS_4$	VI	A	161.6	230.4
$[(C_6H_5)_4P]_2MoOS_3$	VI	A	161.7	230.1
$Mo_2S_4(dtc)_2$[b]	V	A, B	162.3	229.6
$[(C_6H_5)_4P]_2[Mo_2(S_2)_6]$	V		162.6	229.9
$[(C_6H_5)_4P]_4[Mo_2S_2(CN)_8]\cdot 2H_2O$	IV	B	162.4	229.3
$K_6[Mo_2S(CN)_{12}]\cdot 4H_2O$	IV	D	162.9	229.7
$K_5[Mo_3S_4(CN)_9]\cdot 2H_2O$	IV	B, C	162.6	229.9
$K_8[Mo_4S_4(CN)_{12}]\cdot 4H_2O$	III	C	163.2	229.0
$K_6[Mo_2S_2(CN)_8]\cdot 4H_2O$	III	B	162.3	229.5

[a] For definition see Different Types of Mo–S Bonds. [b] dtc = diethyldithiocarbamate.

(30) A. Gołębiewski and H. Kowalski, *Theor. Chim. Acta*, **12**, 293 (1968).
(31) A. Müller, R. Jostes, and F. A. Cotton, *Angew. Chem.*, **92**, 921 (1980); *Angew. Chem., Int. Ed. Engl.*, **19**, 875 (1980).
(32) Trinh-Toan, B. K. Teo, J. A. Ferguson, T. J. Meyer, and L. F. Dahl, *J. Am. Chem. Soc.*, **99**, 408 (1977).

MOs in the case of the Mo complex. The near-IR/vis absorptions are assigned to transitions within the $\{Mo_4\}$ cluster. Their positions and intensities are comparable to those of $\{Mo_3\}$ systems. As all S 3p AOs are involved in Mo–S bonds, there are no sulfur lone pairs in the HOMO region. Thus, no charge-transfer transitions of the type S → Mo can be found in the electronic spectrum. This also leads to a less negative charge on the S atoms, which is in accordance with the relatively high ESCA binding energies of the S 2p electrons (cf. Table XVI). (This effect has also an influence on the IR band intensities of the ν(CN) vibrations.)

(b) $[Mo_3S_4(CN)_9]^{5-}$ (2). Metal–metal bonding in trinuclear clusters of the early transition elements has been discussed on the basis of a simple model.[31] The MO calculation (see Figure 10) confirms the applicability of the model for **2**, resulting in three (occupied) metal–metal bonding orbitals (a_1 and e) as HOMOs and an unoccupied set of metal–metal antibonding orbitals (a_1, e, a_2, e). The character of the unoccupied a_1 MO is particularly interesting, since it determines the redox chemistry of trinuclear clusters of this structural type.[33] In the case of **2** the destabilizing Mo–S π-antibonding character of this orbital is diminished by a strong delocalization to $\pi^*(CN^-)$ orbitals; thus, the cluster is capable of reversible electrochemical reduction (see below).

The composition of the MOs with mainly S 3p character (as in the case of $[Mo_2S_2(CN)_8]^{n-}$) shows appreciable π bonding in the Mo–(μ-S) bonds (d_{av} = 2.322 Å), which is also inferred from the relatively high overlap populations. The calculations as well as our resonance Raman studies (see above) suggest that the lowest energy absorption should be assigned to a transition within the $\{Mo_3\}^6$ system, whereas the absorptions at 26.5 × 10^3 and 29.2 × 10^3 cm^{-1} should be assigned to S → Mo charge-transfer transitions.

(c) $[Mo_2S_2(CN)_8]^{6-}$ (3) and $[Mo_2S_2(CN)_8]^{4-}$ (4). The electronic structure of the $[Mo_2S_2(CN)_8]^{6-}$ ion has been studied before on the basis of a Fenske–Hall calculation.[34] The results could be reproduced qualitatively by our EH calculations, which were also extended to the oxidized species **4**. The rather high Mo 4d participation in the b_{1g} and b_{2u} MOs with predominant S 3p character shows appreciable π bonding. There are two distinctly bonding metal–metal orbitals ($a_g \triangleq \sigma$ bonding, $b_{2u} \triangleq \pi$ bonding) and the approximately nonbonding a_u orbital (δ^*). The unexpected ordering of the δ^*, π, and δ levels (see Figure 11) is caused by the fact that the $b_{1g}(\delta)$ and $b_{2u}(\pi)$ orbitals are strongly π antibonding with respect to the Mo–S bonds, whereas the $a_u(\delta^*)$ orbital has no sulfur s and p participation due to symmetry restrictions. The latter orbital should be regarded as essentially nonbonding because of the relatively small S_δ(Mo4d,Mo4d) overlap integrals at the internuclear distances in **3** and **4**. Both complexes are diamagnetic due to the configurations $\sigma^2\delta^{*2}$ (**4**) and $\sigma^2\delta^{*2}\pi^2$ (**3**).

It should be noted that the ordering of the MOs of the metal–metal bonding system given in Figure 11 is very similar to that found by Hoffmann and co-workers[35] in model calculations on Re_2Cl_{10} at metal–metal distances of ca. 3.15 Å. An electron configuration equal to that of **3** has been proposed for the $\{M_2\}^6$ system $(H_2EDTA)Tc(\mu\text{-}O)_2Tc(H_2EDTA)$.[36]

The given ordering of the MOs is also consistent with the X-ray structure results, as the Mo–Mo bond is longer and the M–S bonds are shorter in **4** compared to those in **3**. The multiple Mo–Mo bond order is nicely demonstrated by the Mo–Mo overlap population, which is much higher than the corresponding ones of **1** and **2** having Mo–Mo single bonds.

The two near-IR/vis absorptions of **3** are due to the $\pi \rightarrow \pi^*$ and $\delta^* \rightarrow \delta$ transitions, whereas the vacancy of a low-lying metal-localized MO in **4** allows a charge-transfer transition of the type S 3p → π (Mo–Mo) from lower S-localized orbitals (intense absorption at 15.2 × 10^3 cm^{-1}; cf. also the discussion of the resonance Raman spectra of **3** and **4**). The other absorptions of **3** and **4** with $\tilde{\nu} < 35 \times 10^3$ cm^{-1} should mainly be caused by charge-transfer transitions of the type S 3p → Mo 4d.

(d) $[Mo_2S(CN)_{12}]^{6-}$ (5). The striking structural feature of this complex is the linear MoSMo unit with an Mo–S distance (2.172 Å)[20] typical for a multiple-bond order. The electronic structure of the complex has already been discussed qualitatively.[11] Our MO calculation (assuming D_{5h} symmetry) yields the MO scheme presented in Figure 12. As was proposed earlier,[37] S 3d orbitals play an important role in the bonding in this complex (in contrast to the case for the other cyanothiomolybdates). Besides the Mo–S–Mo σ-bonding a_2'' orbital there are π-bonding (e_1'), nonbonding (e_1''), and antibonding MOs (e_1'), mainly formed from two S 3p AOs and two 4d AOs of each Mo center. The HOMO (e_1'') is mainly localized on the Mo, and by symmetry restriction the contribution of sulfur is only possible via 3d functions. This orbital is essentially nonbonding, in agreement with the possibility of reversible electrochemical oxidation of the complex at rather low potential.[38]

The intense absorption at 27.0 × 10^3 cm^{-1} has to be assigned to a symmetry-allowed component of the HOMO → LUMO (e_1'' → e_1') transition (with Mo → S charge-transfer character). As there are no other low-lying "Mo 4d" orbitals, the absorption at 16.1 × 10^3 cm^{-1} might be a symmetry-forbidden component of the mentioned transition (as inferred from intensity considerations). However, in disagreement with this suggestion, a resonance Raman experiment (λ_e = 647.1 nm) resulted in an enhancement of the ν(CN) bands (by a factor of ca. 10 compared to a Raman spectrum with λ_e = 488.0 nm), leaving the lower energy Raman bands essentially unaffected. The last observation does not exclude an assignment as a d → d transition, as had been suggested earlier.[11]

Calculations on the complex in different conformations (symmetries D_{5h} with eclipsed and D_{5d} with staggered CN^- ligands, with D_5 between these two) led to almost no variation of the total energies, indicating a very low energy of the rotational barrier.

(e) Comparison of the Metal–Metal Bonding Systems of 1–4. It is interesting to point out some similarities in the molecular and electronic structures of **1–4**. In all four complexes the Mo atoms are coordinated in a pseudooctahedral way. If the different ligands are disregarded, the higher aggregated clusters can formally be constructed by the stepwise addition of ML_3 fragments to the basic M_2L_{10} unit of **3** and **4**. The simplified theoretical procedure outlined in ref 31 for trinuclear clusters thus allows a correlation of the metal–metal bonding systems. If the ligands are taken as pure σ donors (this approximation yields a fair description of metal–metal bonding, although the energy sequence is not in all cases correct), the following correlations are obtained:

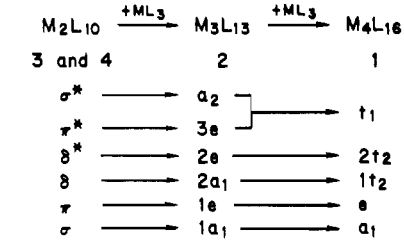

Interestingly, the low potential redox chemistry of **1** and **2** (see below) is governed by related orbitals ($1t_2$ and $2a_1$, respectively), both of which are mainly of the δ type. It may be suggested as a general trend that MOs originating from δ combinations of metal d AOs often make redox reactions possible because of their neither strongly bonding nor antibonding character.

(f) Different Types of Mo–S Bonds. An important feature of Mo–S bonds, in general, is the occurrence of π bonding over a

(33) R. E. McCarley in "Mixed-Valence Compounds", Brown, D. B., Ed., D. Reidel, 1980, p 337.
(34) L. Szterenberg and B. Jeżowska-Trzebiatowska, *Bull. Acad. Pol. Sci., Ser. Sci. Chim.*, **29**, 219 (1981).
(35) S. Shaik, R. Hoffmann, C. R. Fisel, and R. H. Summerville, *J. Am. Chem. Soc.*, **102**, 4555 (1980).
(36) H. B. Bürgi, G. Anderegg, and P. Bläuenstein, *Inorg. Chem.*, **20**, 3829 (1981).
(37) C. Mealli and L. Sacconi, *Inorg. Chem.*, **21**, 2870 (1982).
(38) N. C. Howlader, G. P. Haight, T. W. Hambley, and G. A. Lawrance, *Inorg. Chim. Acta*, **76**, L213 (1983).

wide range of bond lengths (ca. 2.1–2.4 Å), if S 3p lone pairs are available. This is strongly supported by the fact that the overlap integral S_π(Mo4d,S3p) varies to a relatively small extent with the internuclear distance (compared, e.g., to that for Mo–O bonds). Besides, the Mo 4d and S 3p VOIPs are nearly equal. Thus, very different electron density distributions within the Mo–S bonds are possible (dependent on geometry, electron population, and additional ligands).

The structure types A–D (neglecting formal bond orders) have to be considered. The series A–B–C–D is characterized by a

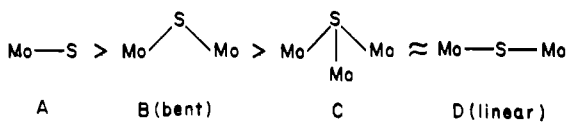

decrease of the negative charge on S (large charge separation, e.g., in MoS_4^{2-}[39] and almost equal net charges of Mo and S in $[Mo_2S(CN)_{12}]^{6-}$). The latter facility of charge displacement should be important for the properties of Mo–S systems in Mo enzymes and their precursors in early evolution.

Charge-transfer bands of the type S → Mo are observed in compounds having structure types A and B but not type C, whereas the opposite transition (Mo → S) is found for type D.

X-ray Photoelectron Spectra. The ESCA data for S 2p and Mo $3d_{5/2}$ for a series of Mo and S compounds including those of the investigated complexes are given in Table XVI.

The Mo $3d_{5/2}$ and the S 2p binding electron energies do not show a clear relation to the oxidation state of the metal. Within this series of compounds the main influence is obviously produced by the number of nearest neighbors to which the sulfide is bound. It is, in principle, possible to distinguish between terminal, doubly bridging, and triply bridging sulfur atoms of complexes having the same oxidation state of Mo. The corresponding binding energies increase in this order and show a spacing of more than 0.5 eV between the different kinds of coordination and may thus be used as an analytical tool. This is in agreement with the results of the MO calculations.

Reversible Redox Reactions, Preparation of Cyanothiomolybdates from Molybdenum Sulfides, and Possible Prebiotic Relevance. The similarities between the model substances for the ferredoxins and the complexes under study regarding their formal electron-transfer properties are striking, since all known cyanothiomolybdates undergo reversible electrochemical redox reactions. While this was shown by Haight et al. for **5**[38] by a CV study according to

$$[Mo_2S(CN)_{12}]^{4-} \underset{+0.05\ V}{\overset{+2e^-}{\underset{-2e^-}{\rightleftharpoons}}} \underset{\mathbf{5}}{[Mo_2S(CN)_{12}]^{6-}} \underset{-2.08\ V}{\overset{+2e^-}{\underset{-2e^-}{\rightleftharpoons}}} [Mo_2S(CN)_{12}]^{8-}$$

(in this and the following reactions, potentials relative to NHE are given below the reaction arrows), we were now able to observe the redox processes (the CV studies on **1** and **2** have been discussed in detail elsewhere;[40] see also ref 41 for other data)

$$\underset{\mathbf{1}}{[Mo_4S_4(CN)_{12}]^{8-}} \underset{+0.275\ V}{\overset{-e^-}{\underset{+e^-}{\rightleftharpoons}}} [Mo_4S_4(CN)_{12}]^{7-} \underset{-0.39\ V}{\overset{-e^-}{\underset{+e^-}{\rightleftharpoons}}} [Mo_4S_4(CN)_{12}]^{6-}$$

$$[Mo_3S_4(CN)_9]^{4-} \underset{+0.455\ V}{\overset{+e^-}{\underset{-e^-}{\rightleftharpoons}}} \underset{\mathbf{2}}{[Mo_3S_4(CN)_9]^{5-}} \underset{-1.49\ V}{\overset{+e^-}{\underset{-e^-}{\rightleftharpoons}}} [Mo_3S_4(CN)_9]^{6-}$$

$$\underset{\mathbf{3}}{[Mo_2S_2(CN)_8]^{6-}} \underset{-1.12/-1.20\ V}{\overset{-2e^-}{\underset{+2e^-}{\rightleftharpoons}}} \underset{\mathbf{4}}{[Mo_2S_2(CN)_8]^{4-}}$$

The possibility of oxidizing **1** reversibly is in accordance with the existence of the clusters $[Mo_4S_4(C_5H_4Pr)_4]^{n+}$ (n = 0, 1, 2)[42] with central Mo_4S_4 units and a formal number of 12, 11, and 10 cluster electrons. Correspondingly, cyclopentadienyl analogues of **2** are known with $\{Mo_3\}^6$ and $\{Mo_3\}^7$ configurations ($[Mo_3S_4Cp_3]^+$[43] and $[Mo_3S_4Cp_3]$[44]). **4** can be obtained from **3** by a two-electron oxidation ($E_{1/2}^{ox}$(**3**) = −1.12 V (in H_2O), $E_{1/2}^{red}$(**4**) = −1.20 V (in Me_2SO)).

These investigations may be of interest for the following reasons. It has been assumed that microorganisms on the early earth were similar to the clostridia (anaerobic, heterotrophic),[2] in which we find not only non-heme iron–sulfur proteins (ferredoxins) but also Mo enzymes. It may, therefore, be assumed that Mo and Fe preenzymes played a vital role in an early stage of evolution (very interesting is the role of Mo: Crick and Orgel[45,46] have argued that the presence of elements in living organisms that are extremely rare on the Earth might indicate that life is extraterrestrial in origin). Some other authors[3,4] have claimed that cyanothiometalates (especially molybdates) were precursors of the metal enzymes and could have been formed by reaction of CN^- with Mo sulfides.

With respect to these facts, it is important to realize that $[Mo_3S_4(CN)_9]^{5-}$ and $[Mo_4S_4(CN)_{12}]^{8-}$ are obtained by reaction of MoS_3 with CN^- in aqueous solution (see Experimental Section). Since the trinuclear cluster can only be obtained from substrates where the Mo_3S_4 triangle is preformed and not by reaction of MoO_4^{2-}, CN^-, and H_2S and since it is produced by the above reaction in very high yield ($[Mo_4S_4(CN)_{12}]^{8-}$ is only a minor (but pure) byproduct), it may be assumed that trinuclear cluster units or multiples of it are already present in the X-ray amorphous MoS_3. "Strong" Mo–S–Mo bridges are cleaved only by very high concentrations of CN^-. The trinuclear cluster is also obtained by the cyanolysis of the mineral jordisite (noncrystalline MoS_2), which allows the conclusion that this material correspondingly contains preformed Mo_3 units.

It can be concluded that the reaction of MoS_x and $MMoS_x$ phases with CN^- can give some information about their structures.

Acknowledgment. We thank the Deutsche Forschungsgemeinschaft, the Fonds der Chemie, and the Minister für Wissenschaft und Forschung (NRW) for financial support.

Appendix

The iterative extended Hückel calculations were carried out with a modified version of the EHT-SPD program[47] using the following parameters: geometries from X-ray studies[6,7,10,20] (with idealized symmetries: T_d for **1**, C_{3v} for **2**, D_{2h} for **3** and **4**, D_{5h} for **5**), Clementi's basis functions for neutral atoms[48] (single ζ for Mo 5s, S 3s, C 2s, N 2s; double ζ for Mo 4d, S 3p, C 2p, N 2p), the Mo 5p basis function of Basch and Gray,[49] the VOIP parameters of Baranovskii and Nikol'skii for Mo,[50] the VOIP parameters of Basch, Viste, and Gray for S, C, and N,[51] and the modified Wolfsberg–Helmholz formula[52] for the off-diagonal elements H_{ij} with k = 1.75. Iterative extended Hückel calculations on negative ions give doubtful results,[53] if the H_{ii}'s of all atoms are iterated at the same time. Thus, we carried out an iterative

(39) R. Kebabcioglu and A. Müller, *Chem. Phys. Lett.*, **8**, 59 (1971).
(40) K. Wieghardt, W. Herrmann, A. Müller, W. Eltzner, and M. Zimmermann, *Z. Naturforsch., B: Anorg. Chem., Org. Chem.*, **39B**, 876 (1984).
(41) N. C. Howlader, G. P. Haight, T. W. Hambley, G. A. Lawrance, K. M. Rahmoeller, and M. R. Snow, *Aust. J. Chem.*, **36**, 377 (1983).
(42) J. A. Bandy, C. E. Davies, J. C. Green, M. L. H. Green, K. Prout, and D. P. S. Rodgers, *J. Chem. Soc., Chem. Commun.*, 1395 (1983).
(43) P. J. Vergamini, H. Vahrenkamp, and L. F. Dahl, *J. Am. Chem. Soc.*, **93**, 6327 (1971).
(44) W. Beck, W. Danzer, and G. Thiel, *Angew. Chem.*, **85**, 625 (1973); *Angew. Chem., Int. Ed. Engl.*, **12**, 582 (1973).
(45) F. H. C. Crick, "Life Itself: Its Origin and Nature", Simon and Schuster, New York, 1981.
(46) Cf. R. E. Dickerson, *Sci. Am.*, **239** (3), 62 (1978).
(47) P. Dibout, *QCPE*, No. **256** (1976).
(48) E. Clementi and C. Roetti, *At. Data Nucl. Data Tables*, **14**, 177 (1974).
(49) H. Basch and H. B. Gray, *Theor. Chim. Acta*, **4**, 367 (1966).
(50) V. I. Baranovskii and A. B. Nikol'skii, *Teor. Eksp. Khim.*, **3**, 527 (1967).
(51) H. Basch, A. Viste, and H. B. Gray, *Theor. Chim. Acta*, **3**, 458 (1965).
(52) J. H. Ammeter, H.-B. Bürgi, J. C. Thibeault, and R. Hoffmann, *J. Am. Chem. Soc.*, **100**, 3686 (1978).
(53) A. Viste and H. B. Gray, *Inorg. Chem.*, **3**, 1113 (1964).

calculation on HCN first and adopted the obtained H_{ii}'s (C 2s, 180.9×10^3 cm^{-1}; C 2p, 92.7×10^3 cm^{-1}; N 2s, 206.9×10^3 cm^{-1}; N 2p, 93.7×10^3 cm^{-1}) for the calculations on the actual complexes, only iterating the H_{ii}'s of Mo and S. The influence of S 3d orbitals was tested by using the optimized orbital exponent 1.7077[54] and the VOIP parameters of McGlynn et al.[55]

(54) F. P. Boer and W. N. Lipscomb, *J. Chem. Phys.*, **50**, 989 (1969).
(55) S. P. McGlynn, L. G. Vanquickenborne, M. Kinoshita, and D. G. Carroll, "Introduction to Applied Quantum Chemistry", Holt, Rinehart and Winston, New York, 1972.

Registry No. **1a**, 97278-52-9; **2a**, 72609-97-3; **2b**, 97278-54-1; **2c**, 97278-53-0; **3a**, 71934-12-8; **4a**, 97278-56-3; **4b**, 97278-61-0; **5a**, 25531-12-8; **6a**, 97278-57-4; $[(C_6H_5)_4P]_2MoS_4$, 14348-10-8; $[(C_6H_5)_4P]_2MoOS_3$, 83061-15-8; $Mo_2S_4(dtc)_2$, 36539-27-2; $[(C_6H_5)_4P]_2[Mo_2(S_2)_6]$, 97278-59-6; $NH_4K[Mo_4(NO)_4(S_2)_6O]$, 97278-60-9; $K_8[Mo_4S_4(NO)_4(CN)_8]$, 97335-14-3; S, 7704-34-9; Mo, 7439-98-7.

Supplementary Material Available: Thermal parameters (Tables SI and SIII) and structure factor amplitudes (Tables SII and SIV) for **2b** and **4b** (23 pages). Ordering information is given on any current masthead page.

Contribution from the Department of Chemistry and Geology, Clemson University, Clemson, South Carolina 29634

Solid-State and Solution Properties of (*N*,*N*′-Ethylenebis(salicylideneaminato))(nitrato)iron(III) and Related Complexes

JAMES C. FANNING,* JAMES L. RESCE, GARY C. LICKFIELD, and MARGARET E. KOTUN

Received August 3, 1984

Two solid-state forms of the title complex, $Fe(salen)NO_3$, were prepared by reacting a methylene chloride solution of $[Fe(salen)]_2O$ with aqueous 0.5 M nitric acid and precipitating the complex either with ether or with pentane. The form isolated from pentane was dimeric with a unidentate nitrate bound to each iron, $[Fe(salen)ONO_2]_2$, while the other form was monomeric with a bidentate nitrate, $Fe(salen)O_2NO$. The reaction was carried out with three other salicylideneamine iron(III) μ-oxo complexes, and only the dimeric, unidentate nitrate form of each was prepared. The ^{15}N-labeled nitrate complexes were used to assign the nitrate infrared bands. The ^{57}Fe Mössbauer spectra and magnetic susceptibilities of the complexes were compared to similar data for the tetraphenylporphyrin complex $Fe(TPP)O_2NO$, which is monomeric with a bidentate nitrate. The proton NMR spectra of the two forms of $Fe(salen)NO_3$ in solution were identical, as were the solution infrared spectra, and such spectra indicated that the solution species were monomeric with bidentate nitrate ligands.

Introduction

Iron nitrate complexes have only been studied to a limited extent,[1-5] even though a wide variety of other metal nitrate complexes have been reported and used to describe the binding of nitrate to metal ions.[6-10] Of the iron nitrates known, most are iron(III) since iron(II) is expected to reduce nitrate.[11] However, $(C_5H_5)Fe(CO)_2(NO_3)$, with iron in a reduced oxidation state, has been reported[12] and its structure shows a unidentate-bound nitrate.[5] Recent experiments have pointed out a need for more information on iron(III) nitrates.

A methylene chloride solution of $[Fe(salen)]_2O$[13] has been shown recently[14] to react rapidly with nitric oxide and dioxygen to produce, upon solvent removal, a fine black powder with the apparent formula $Fe(salen)NO_3$. The black powder has proven to be an interesting material since it can serve as a powerful nitrosating agent.[14] When heated with a methylene chloride or toluene solution containing a secondary amine, such as pyrrolidine or morpholine, the powder produced a high yield of the carcinogenic *N*-nitrosamine. Because of the possible involvement of the biologically important species iron and nitrate in *N*-nitrosamine production, the black powder and the nitrosation reactions are under study at this time. In order to proceed with this study, it was necessary to have some detailed information on iron(III) salicylideneamine nitrate complexes.

Since there was some uncertainty about the nature of the black powder, a more direct preparative procedure for the iron(III) salicylideneamine nitrates was needed. The iron(III) nitrate, $Fe(TPP)O_2NO$, described by Goff and co-workers,[1] were prepared by reacting a methylene chloride solution of $[Fe(TPP)]_2O$ with an aqueous 6 M nitric acid solution and isolating the product from the organic layer. When we reacted a methylene chloride solution of $[Fe(salen)]_2O$ with dilute nitric acid and varied the conditions of product isolation, two different nitrate complexes were obtained. One appeared to be dimeric, similar to $[Fe(salen)Cl]_2$,[15] while the other was like $Fe(TPP)O_2NO$—monomeric with a bidentate nitrate.[1] Below, these and other salicylideneamine iron(III) nitrate complexes are discussed and compared with $Fe(TPP)O_2NO$.

Experimental Section

Chemicals. All reagents and solvents were reagent grade. Methylene chloride and toluene were purified by standard procedures.[16] Salicylaldehyde was vacuum distilled, and ethylenediamine and propylenediamine were vaccum distilled from KOH. The salicylideneamine ligands (H_2L) were prepared by reacting two parts of the salicylaldehyde with

(1) Phillipi, M. A.; Baenziger, N.; Goff, H. M. *Inorg. Chem.* **1981**, *20*, 3904.
(2) King, T. J.; Logan, N.; Morris, A.; Wallwork, S. C. *J. Chem. Soc., Chem. Commun.* **1971**, 554.
(3) Addison, C. C.; Boorman, P. M.; Logan, N. J. *J. Chem. Soc.* **1965**, 4978, 5146.
(4) Campbell, M. J.; Grzeskowiak, M. R.; Juneju, G. S. *J. Inorg. Nucl. Chem.* **1978**, *40*, 1507.
(5) Struchkov, Yu. T.; Alexsandrov, G. G.; Kaganovich, V. S.; Rybinskaya, M. I. *Koord. Khim.* **1981**, *7*, 949.
(6) Critchlow, P. B.; Robinson, S. D. *Coord. Chem. Rev.* **1978**, *25*, 69.
(7) Addison, C. C.; Logan, N.; Wallwork, S. C.; Garner, C. D. *Q. Rev., Chem. Soc.* **1971**, *25*, 289.
(8) Addison, C. C.; Sutton, D. *Prog. Inorg. Chem.* **1967**, *8*, 195.
(9) Addison, C. C.; Logan, N. *Adv. Inorg. Chem. Radiochem.* **1964**, *6*, 72.
(10) Field, B. O.; Hardy, C. J. *Q. Rev., Chem. Soc.* **1964**, *18*, 361.
(11) Epstein, I. R.; Kustin, K.; Warshaw, L. J. *J. Am. Chem. Soc.* **1980**, *102*, 3751.
(12) Johnson, E. C.; Meyer, T. J.; Winterton, N. *Inorg. Chem.* **1971**, *10*, 1673.
(13) Abbreviations: salicylideneamine ligands (H_2L) H_2salen, *N*,*N*′-ethylenebis(salicylideneamine); H_2salpn, *N*,*N*′-propylenebis(salicylideneamine); H_2(5-Clsalen), *N*,*N*′-ethylenebis(5-chlorosalicylideneamine); H_2(5-MeOsalen), *N*,*N*′-ethylenebis(5-methoxysalicylideneamine); porphyrin ligand H_2TPP, *meso*-tetraphenylporphyrin.
(14) Croisy, A. F.; Fanning, J. C.; Keefer, L. K.; Slavin, B. W.; Uhm, S.-J. *IARC Sci. Publ.* **1980**, *No. 31*, 83–93.
(15) Gerloch, M.; Mabbs, F. E. *J. Chem. Soc. A* **1967**, 1900.
(16) Gordon, A. J.; Ford, R. A. "The Chemist's Companion"; Wiley: New York, 1972; p 430 ff.

0020-1669/85/1324-2884$01.50/0